3D). Flow cytometric analyses revealed that the percentage of Dlk^+ cells in wild-type colonies was 0.9% ± 0.2% at day 7 and 0.5% ± 0.1% at day 14 of culture, although that in *Ink4a/Arf*$^{-/-}$ colonies was 8.6% ± 0.7% and 4.5% ± 0.3%, respectively (Fig. 3E). These findings indicate the enhanced self-renewal capability of hepatic stem cells on the loss of *Ink4a/Arf* expression. Of note, messenger RNA expression of *Bmi1* was comparable between wild-type and *Ink4a/Arf*$^{-/-}$ Dlk^+ cells (data not shown).

As expected, but importantly, the ability of wild-type Dlk^+ cells to propagate colonies was extremely compromised by cotransduction with *Ink4a* and *Arf* retroviruses. Immunocytochemical analyses and flow cytometric analyses showed that the Dlk^+ fraction and bipotent cells were significantly reduced in culture (Supporting Fig. 4).

Enhanced Self-Renewal of Ink4a/Arf$^{-/-}$ Hepatic Stem Cells by Bmi1 Overexpression. We previously reported that forced expression of *Bmi1* enhances the self-renewal capacity of hepatic stem/progenitor cells and eventually induces their transformation.[3] To elucidate whether the functional significance of Bmi1 is attributable to the repression of *Ink4a/Arf*, we performed gain-of-function assays of *Bmi1* in *Ink4a/Arf*$^{-/-}$ cells. *Ink4a/Arf*$^{-/-}$ Dlk^+ cells were transduced with either control enhanced green fluorescent protein (*EGFP*) or *Bmi1* 12-18 hours after purification. Enforced expression of Bmi1 was verified by western blot analysis (Fig. 4A). Exogenous Bmi1 in *Ink4a/Arf*$^{-/-}$ Dlk^+ cells did not significantly increase colony number (Fig. 4B). Of note, however, the diameter of *Bmi1*-overexpressing colonies was significantly larger than that of the control colonies (Fig. 4C). Furthermore, flow cytometric analyses showed that the percentage of *Ink4a/Arf*$^{-/-}$ Dlk^+ cells labeled with EGFP was higher in *Bmi1* cultures than in control cultures (22.6% ± 2.3%, 14.0% ± 1.2%, and 8.8% ± 0.7% versus 8.4% ± 1.1%, 3.4% ± 0.5%, and 2.1% ± 0.2% at days 7, 14, and 28 of culture, respectively) (Fig. 4D).

We next carried out single-cell sorting of Dlk^+ cells contained in primary colonies at days 14 and 28 of culture in order to evaluate their self-renewal capacity in terms of replating activity. Dlk^+ cells overexpressing *Bmi1* gave rise to 3.1-fold to 4.0-fold more secondary colonies than the control (Fig. 5A). Secondary colonies were generated in a similar fashion to the original colonies. Immunocytochemical analyses demonstrated that the frequency of Alb^+CK7^+ bipotent cells was significantly higher in secondary colonies derived from Dlk^+ cells collected from the primary *Bmi1*-transduced *Ink4a/Arf*$^{-/-}$ colonies at days 14 and 28 of culture (Fig. 5B,C).

In contrast, *Bmi1*$^{-/-}$*Ink4a/Arf*$^{-/-}$ Dlk^+ cells behaved like *Ink4a/Arf*$^{-/-}$ Dlk^+ cells (Supporting Fig. 5). Although loss of Bmi1 still affected the function of *Ink4a/Arf*$^{-/-}$ hepatic stem/progenitor cells to some extent, these findings indicate that *Ink4a/Arf* is the major target of Bmi1 in hepatic stem cells as in HSCs and NSCs.

Acquisition of Tumorigenic Capacity by Bmi1-Transduced Ink4a/Arf$^{-/-}$ Hepatic Stem Cells. We then tested whether the loss of both *Ink4a* and *Arf* is enough for the transformation of hepatic stem cells. Considering that a large number of cells were necessary for transplantations assays, these cells were allowed to form colonies in culture for 28 days. Immunocytochemical analyses showed that more than 90% of cells transduced with *Bmi1* expressed both EGFP, a marker antigen for retrovirus integration, and Flag-tagged Bmi1 (Supporting Fig. 6). Subsequently, a total of 2×10^6 transduced cells were transplanted into the subcutaneous space of NOD/SCID mice (Fig. 5D). Although all the mice transplanted with *Bmi1*-transduced *Ink4a/Arf*$^{-/-}$ Dlk^+ cells developed tumors, none of those transplanted with control *Ink4a/Arf*$^{-/-}$ Dlk^+ cells did. Histological analyses revealed that the subcutaneous tumors consisted of both Alb^+ parenchymal cells and a $CK7^+$ glandular structure (Fig. 5D). The histological finding is consistent with our previous observation in tumors derived from *Bmi1*-transduced wild-type hepatic stem cells.[3] These findings clearly indicate that repression of the *Ink4a* and *Arf* genes is not enough for Bmi1 to achieve its tumorigenic potential in hepatic stem cells.

Gene Expression Analyses of Bmi1-Transduced Ink4a/Arf$^{-/-}$ Hepatic Stem Cells. In order to explore novel targets for Bmi1, *Ink4a/Arf*$^{-/-}$ Dlk^+ cells were infected with either the control *EGFP* or *Bmi1*-expressing retrovirus and allowed to form colonies. Dlk^+ cells were purified from colonies at day 28 of culture by cell sorting and subjected to gene expression profiling using oligonucleotide microarrays. We selected genes exhibiting a twofold or greater change with statistical significance in *Bmi1*-transduced *Ink4a/Arf*$^{-/-}$ Dlk^+ cells compared to control *Ink4a/Arf*$^{-/-}$ Dlk^+ cells. As a result, we identified 75 down-regulated genes and 97 up-regulated genes in total (Supporting Table 1). Functional annotation based on GO showed significant enrichment for down-regulated genes which fell into the category "metabolism" and "transport", which included many hepatocyte maturation genes (Fig. 6A). This indicates that Bmi1 strongly suppresses the differentiation and maturation of hepatocytes.

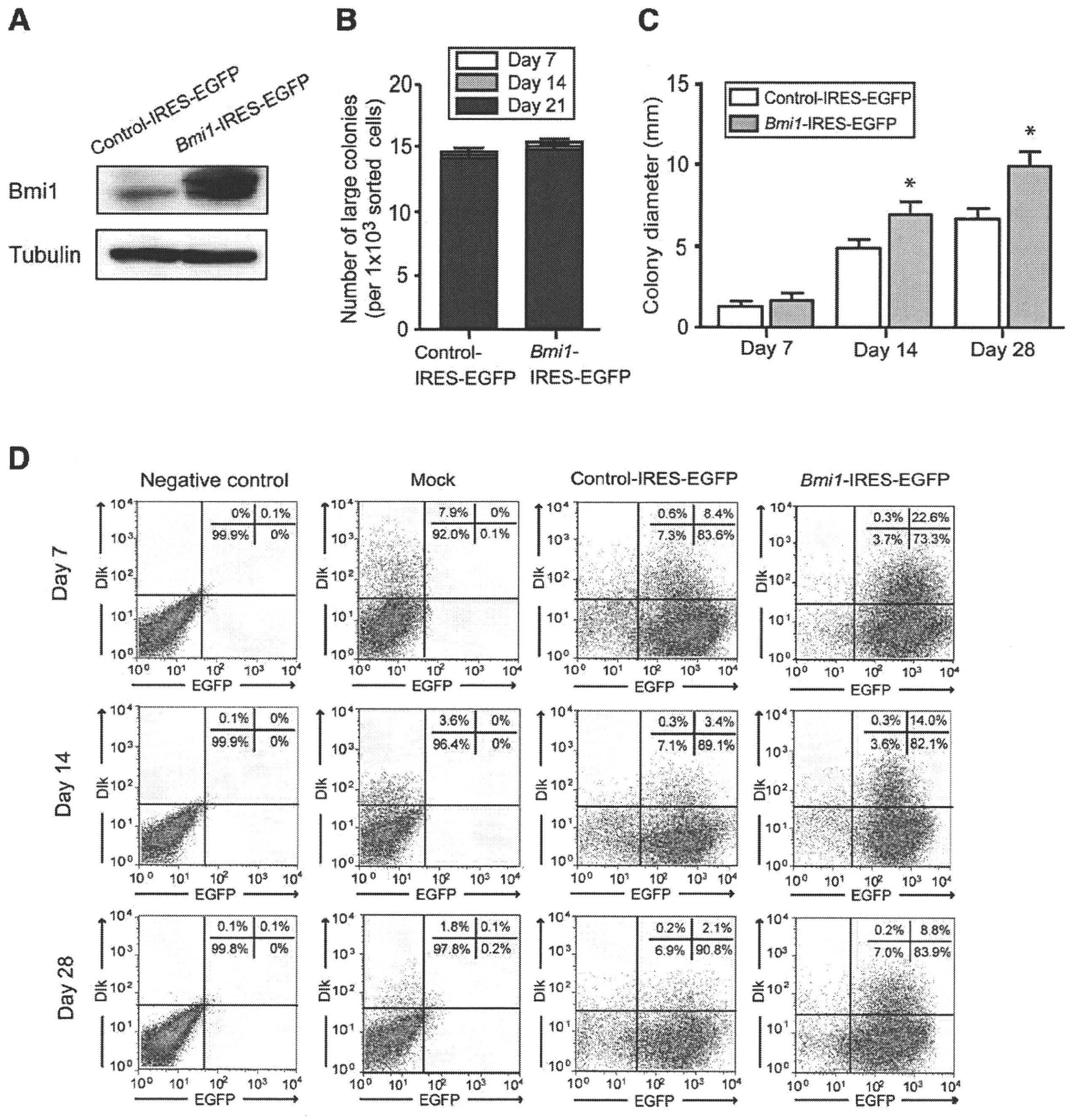

Fig. 4. Gain-of-function assays of *Bmi1* in *Ink4a/Arf*$^{-/-}$ Dlk$^+$ cells. (A) Cells transduced with indicated retroviruses were subjected to western blot analysis using anti-Bmi1 and anti-tubulin (loading control) antibodies. (B) The number of large colonies containing more than 100 cells at day 7 of culture was traced up to day 21. (C) The diameter of colonies at days 7, 14, and 28 after transduction of indicated retroviruses. *Statistically significant ($P < 0.05$). (D) Flow cytometric profiles of colonies derived from nontransduced (mock) and *EGFP* or *Bmi1*-transduced *Ink4a/Arf*$^{-/-}$ Dlk$^+$ cells at days 7, 14, and 28 in culture. The percentages of each fraction are shown as mean values for three independent analyses.

Recent whole-genome ChIP-on-chip analyses successfully identified genes that are bound by PRC1 and PRC2 complexes in embryonic stem cells (ESCs).[19-21] Boyer et al. reported the genes occupied by PRC1 (Phc1 and Rnf2) and PRC2 (Suz12 and Eed) in murine ESCs.[19] To explore a novel target of Bmi1 in hepatic stem/progenitor cells, we compared the list of down-regulated genes with the ChIP-on-chip data documented by Boyer et al.[19] As a result, five genes namely, *Sox17*, *Irx5*, *Gjb2*, *Shox2*, and *Bhmt2* in the present study appeared to be regulated by both PRC1 and/or PRC2 in ESCs (Fig. 6B). We therefore considered these genes as candidates for direct targets of Bmi1 in hepatic stem cells and performed further analyses on them. In order to confirm the altered expression of these 5 candidate genes, *Ink4a/Arf*$^{-/-}$ Dlk$^+$

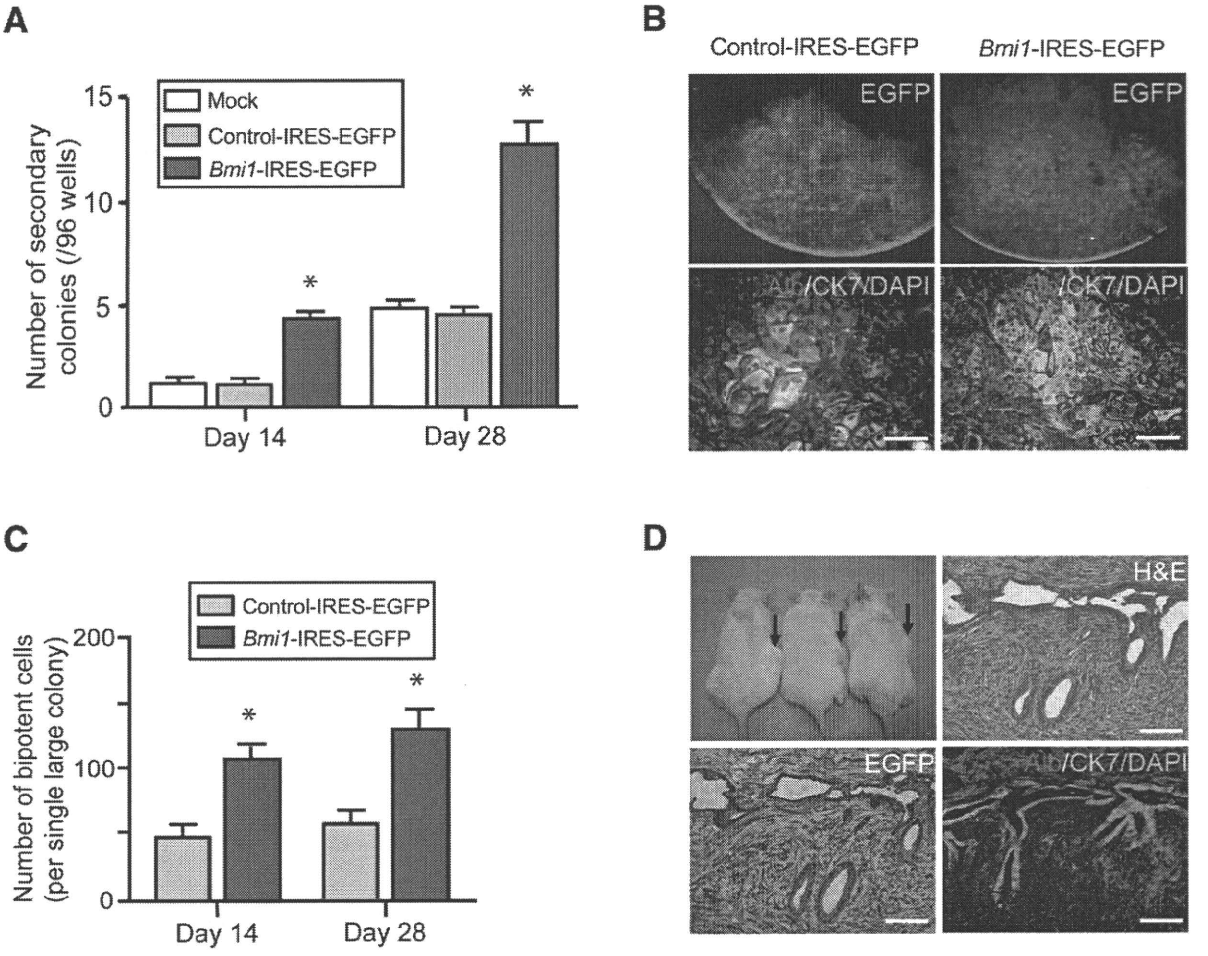

Fig. 5. Replating assays and implantation of *Bmi1*-transduced *Ink4a/Arf*$^{-/-}$ Dlk$^+$ cells. (A) Dlk$^+$ cells in primary colonies generated from nontransduced (mock) and *EGFP* or *Bmi1*-transduced *Ink4a/Arf*$^{-/-}$ Dlk$^+$ cells were clone-sorted at days 14 and 28 of culture and allowed to form colonies. The replating efficiency of Dlk$^+$ cells was evaluated by counting the number of secondary colonies containing more than 100 cells 14 days after replating by clone-sorting. *Statistically significant ($P < 0.05$). (B) Fluorescence images (upper panels) and dual immunostaining (lower panels) of secondary clonal colonies derived from *EGFP* or *Bmi1*-transduced *Ink4a/Arf*$^{-/-}$ Dlk$^+$ cells at day 28 of culture. Alb (red) and CK7 (green) expression in secondary colonies was merged with nuclear DAPI staining (blue). Scale bar = 100 μm. (C) The absolute number of Alb$^+$CK7$^+$ bipotent cells in secondary large colonies at day 14 of subculture. *Statistically significant ($P < 0.05$). (D) *Ink4a/Arf*$^{-/-}$ Dlk$^+$ cells were transduced with the control *EGFP* or *Bmi1*-expressing retrovirus and a total of 2×10^6 transduced cells were transplanted into the subcutaneous space of NOD/SCID mice. *Bmi1*-transduced *Ink4a/Arf*$^{-/-}$ cells formed tumors in the right subcutaneous space of recipient mice (arrows), whereas the same number of control *EGFP*-transduced *Ink4a/Arf*$^{-/-}$ cells did not generate tumors in the left space. Hematoxylin and eosin (H&E) staining of tumors demonstrated histological features compatible with combined hepatocellular and cholangiocellular carcinoma. Immunohistochemical analysis revealed that the tumors were positive for EGFP and consisted of Alb$^+$ parenchymal cells (red) and CK7$^+$ glandular structures (green). Scale bar = 200 μm.

cells transduced with either control *EGFP* or *Bmi1* were purified from colonies at day 28 of culture and subjected to real-time RT-PCR analyses. The selected five genes exhibited similar expression profiles as in the microarray analysis in *Ink4a/Arf*$^{-/-}$ Dlk$^+$ cells (Fig. 6C). Forced expression of *Bmi1* in wild-type Dlk$^+$ cells significantly repressed the expression of these genes in a similar fashion to that in *Ink4a/Arf*$^{-/-}$ Dlk$^+$ cells (Fig. 6C).

Gain-of-Function Assays of Sox17 in Hepatic Stem Cells. Among candidates for Bmi1 targets, *sex determining region Y-box 17* (*Sox17*) was most severely down-regulated following *Bmi1*-overexpression in hepatic stem cells (Fig. 6C). It has been reported that *Sox17* is highly expressed in the very early definitive endoderm[22] and in hepatocyte-like cells derived from ESCs.[23] These findings prompted us to further examine the role of *Sox17* in hepatic stem cell self-renewal and tumorigenesis. ChIP assays in wild-type Dlk$^+$ cells demonstrated specific binding of Bmi1 and an increased level of H2Aub1 at the *Sox17* promoter only in cells transduced with the *Bmi1* retrovirus (Fig. 7A).

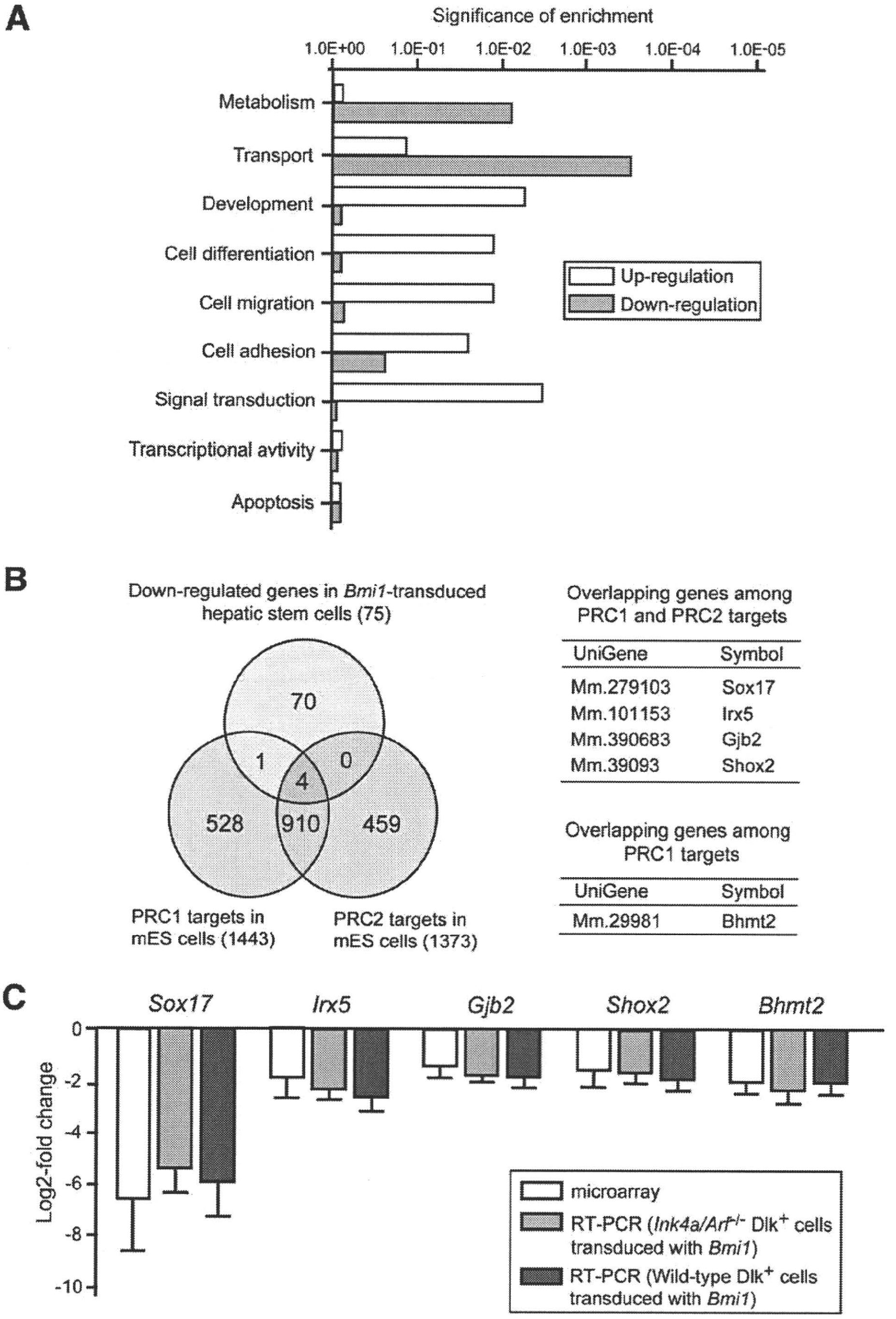

Overlapping genes among PRC1 and PRC2 targets

UniGene	Symbol
Mm.279103	Sox17
Mm.101153	Irx5
Mm.390683	Gjb2
Mm.39093	Shox2

Overlapping genes among PRC1 targets

UniGene	Symbol
Mm.29981	Bhmt2

Fig. 6. Gene expression profiles of *Bmi1*-transduced *Ink4a/Arf*$^{-/-}$ Dlk$^+$ cells. (A) Gene Ontology (GO) analyses of differentially expressed genes. (B) The overlap of down-regulated genes in the present analysis and PRC targets identified by ChIP-on-chip analyses in mouse ESCs[27] are depicted in a Venn diagram (left panel) and in tables at right. (C) Wild-type and *Ink4a/Arf*$^{-/-}$ Dlk$^+$ cells were infected with either the control *EGFP* or *Bmi1*-expressing retrovirus and allowed to form colonies. Dlk$^+$ cells were purified from these colonies at day 28 of culture and subjected to real-time RT-PCR analysis. The messenger RNA expression of candidate genes in *Bmi1*-overexpressing cells was compared to that in control cells. The data obtained by microarray analyses are also presented.

All these findings indicate that Bmi1 could directly regulate the expression of *Sox17*.

We next tested the effect of Sox17 in a gain-of-function assay. Overexpression of Sox17 was confirmed by western blotting (Fig. 7B). Enforced expression of *Sox17* in wild-type Dlk$^+$ cells severely impaired the formation of colonies and reduced the number as well as size of colonies (Fig. 7C,D). Dlk$^+$ cells transduced with *Sox17* did not form any large colonies containing more than 100 cells at day 7 of culture (Fig. 7C) and no colonies expanded beyond day 14 of culture (data not shown). Immunocytochemical analyses showed a decrease in number of Alb$^+$CK7$^+$ bipotent cells in colonies derived from Dlk$^+$ cells transduced with *Sox17* compared to the control colonies (Fig. 7D,E). Concordant with this, flow cytometric analyses demonstrated that the Dlk$^+$ fraction in *Sox17*-transduced colonies was 0.3% ± 0.1%, much lower that that in wild-type colonies (0.9% ± 0.2%) (Fig. 7F).

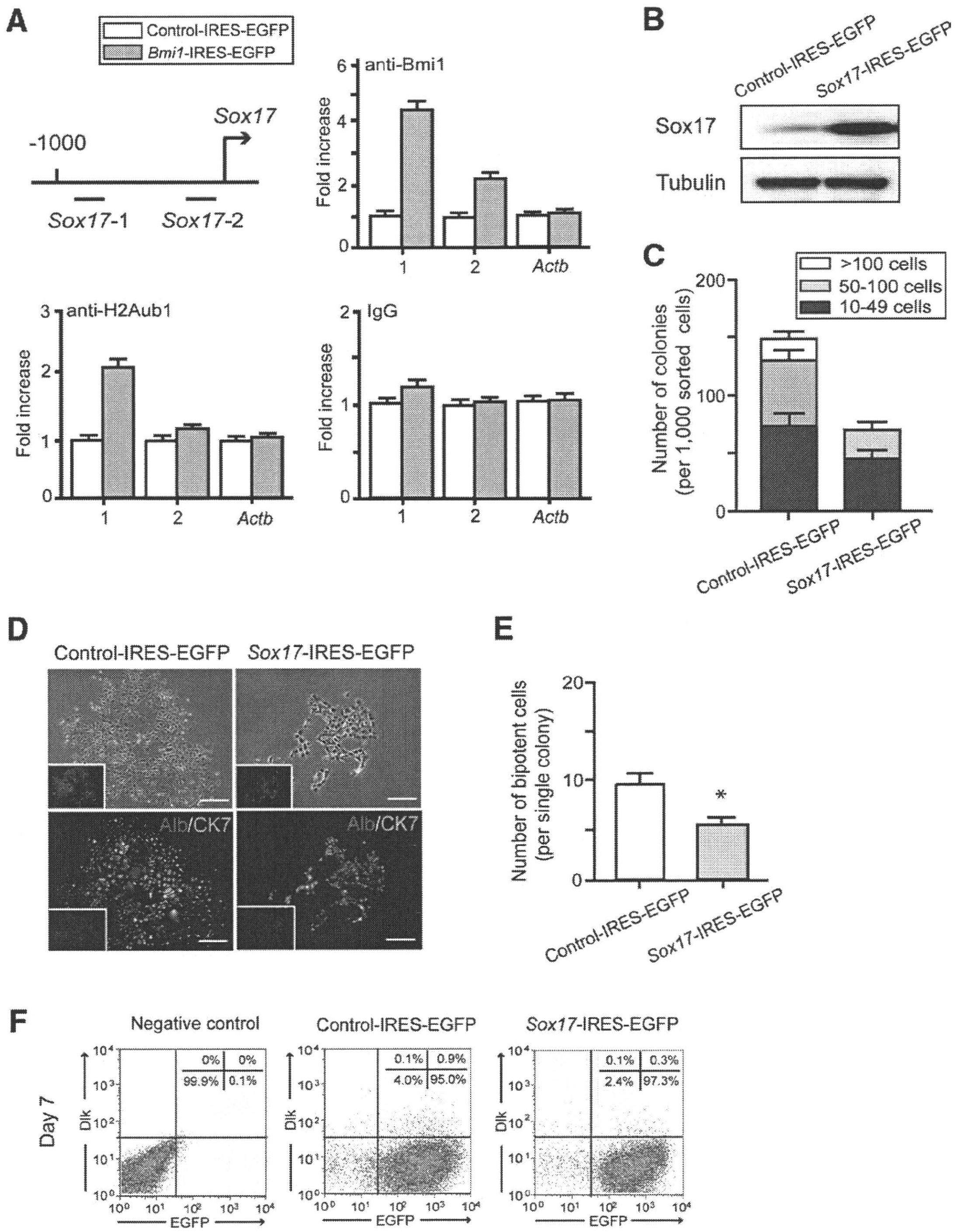

Fig. 7. Gain-of-function assay of *Sox17* in wild-type Dlk$^+$ cells. (A) ChIP analyses of wild-type Dlk$^+$ cells transduced with *EGFP* or *Bmi1* on the *Sox17* locus and *Actb* control promoter region using anti-Bmi1 and anti-H2Aub1 antibodies. *Statistically significant ($P < 0.05$). (B) Western blot analysis in *Sox17*-transduced wild-type Dlk$^+$ cells using anti-Sox17 and anti-tubulin (loading control) antibodies. (C) Enforced expression of *Sox17* in wild-type Dlk$^+$ cells markedly decreased both the total number of colonies and the number of large colonies containing more than 100 cells at day 7 of culture. *Statistically significant ($P < 0.05$). (D) Bright-field images and immunocytochemical analyses of colonies derived from wild-type Dlk$^+$ cells transduced with *Sox17* at day 7 of culture. Alb (red) and CK7 (green) expression was merged. Nuclear DAPI staining (blue) is shown in the insets. Scale bar = 200 μm. (E) The absolute number of Alb$^+$CK7$^+$ bipotent cells in colonies derived from wild-type Dlk$^+$ cells transduced with *Sox17* at day 7 of culture. *Statistically significant ($P < 0.05$). (F) Flow cytometric profiles of colonies derived from *EGFP* or *Sox17*-transduced wild-type Dlk$^+$ cells at day 7 of culture. The percentages of each fraction are shown as mean values for three independent analyses.

To elucidate the impact of *Sox17* on the tumorigenic process driven by *Bmi1*-overexpressing hepatic stem cells, we cotransduced *Ink4a/Arf*$^{-/-}$ Dlk$^+$ cells with *Bmi1* and *Sox17*. *Ink4a/Arf*$^{-/-}$ Dlk$^+$ cells were simultaneously transduced with *Sox17*-IRES-EGFP and *Bmi1*-IRES-Kusabira-Orange (KO)-expressing retroviral vectors (Supporting Fig. 7A). Flow cytometric profiles demonstrated that more than 90% of cells were successfully cotransduced (Supporting Fig. 7B). A total of 2 × 10^6 *Ink4a/Arf*$^{-/-}$ cells cotransduced with *Bmi1* and *Sox17* or control *EGFP* were transplanted into the subcutaneous space of NOD/SCID mice. Cotransduction of *Bmi1* and *Sox17* resulted in a significant reduction in tumor volume compared to the cotransduction of *Bmi1* and control *EGFP* (Supporting Fig. 6C). This result indicates that *Sox17* suppresses the tumorigenic activity of *Bmi1*-overexpressing hepatic stem cells.

We then further tested the effect of *Sox17* knockdown in wild-type Dlk$^+$ cells (Supporting Fig. 8). *Sox17* knockdown mildly promoted colony expansion and increased the Dlk$^+$ fraction and the number of bipotent cells, although its effect was not statistically significant. Transplantation of 2 × 10^6 *Sox17*-knockdown Dlk$^+$ cells did not develop subcutaneous tumors in NOD/SCID mice at all (data not shown).

Discussion

Bmi1, a component of PRC1, regulates the cell cycle, apoptosis and senescence by repressing the *Ink4a/Arf* locus.[5,10] p19^{Arf} suppresses MDM2, which mediates ubiquitin-dependent degradation of p53, and subsequently activates p53 target genes involved in cell cycle arrest and apoptosis, including *p21*.[24] Direct binding of p16^{Ink4a} to CDK4 and CDK6 keeps Rb hypophosphorylated. Hypophosphorylated Rb represses E2F-dependent transcription leading to cell cycle arrest and senescence.[24] Thus, the repression of the *Ink4a/Arf* locus by Bmi1 has a great impact on the maintenance of self-renewing stem cells.

In the present study, *Bmi1*$^{-/-}$ hepatic stem cells showed high levels of *Ink4a* and *Arf* expression and significantly but modestly impaired colony expansion and self-renewal in culture. Although *Bmi1*$^{-/-}$ liver is functionally and histologically normal,[15] oval cell induction following DDC treatment was apparently impaired in *Bmi1*$^{-/-}$ mice (Supporting Fig. 3). Considering the results of gain-of-function (Supporting Fig. 2) and loss-of-function assays of *Bmi1* (Fig. 1), the possibility exists that redundancy among other PcG molecules such as Mel18 weakens the phenotype of *Bmi1*$^{-/-}$ hepatic stem cells in developing and adult liver.[25] In clear contrast, *Ink4a/Arf*$^{-/-}$ hepatic stem cells exhibited enhanced colony formation and retained a large Dlk$^+$ population in culture compared to the wild type. Furthermore, deletion of both *Ink4a* and *Arf* largely restored the impaired self-renewal capacity of *Bmi1*$^{-/-}$ hepatic stem cells (Supporting Fig. 5). These findings indicate that *Ink4a/Arf* is the major target of Bmi1 in hepatic stem cells as in HSCs and NSCs.[11,12]

Bmi1 is also essential for cancer stem cells as demonstrated in a mouse leukemia model as well as in a mouse lung tumor model generated by the expression of a mutant K-ras gene in bronchioalveolar stem cells.[5,26] In addition, we previously demonstrated that forced expression of *Bmi1* promotes the self-renewal of hepatic stem/progenitor cells and contributes to malignant transformation.[3] All these findings highlight the important role of Bmi1 in both the development and maintenance of cancer stem cell systems. Of interest, an *Ink4a/Arf*-independent contribution of Bmi1 to not only self-renewal in neural stem cells but also tumorigenesis in a mouse model for glioma has been reported.[27,28] The current *in vivo* transplant assays ascertained that *Bmi1*-transduced *Ink4a/Arf*$^{-/-}$ Dlk$^+$ cells but not control *Ink4a/Arf*$^{-/-}$ Dlk$^+$ cells acquire tumorigenic potential. *Bmi1*-transduced *Ink4a/Arf*$^{-/-}$ Dlk$^+$ cells showed an augmented self-renewal capability as evident from the higher replating efficiency in the single cell-sorting analysis compared to *Ink4a/Arf*$^{-/-}$ Dlk$^+$ cells. These results clearly demonstrated that repression of the *Ink4a/Arf* locus only does not directly drive tumor initiation in hepatic stem cells. Considering that *Ink4a/Arf*$^{-/-}$ mice barely developed primary liver tumors in their lifetime,[29] repression of additional targets of *Bmi1* may be needed in cancer initiation.

To evaluate the impact of Bmi1 on gene expression in hepatic stem cells and to explore the additional targets of Bmi1 related to tumorigenesis, we conducted an oligonucleotide array analysis using *Bmi1*-transduced *Ink4a/Arf*$^{-/-}$ Dlk$^+$ cells and the control *Ink4a/Arf*$^{-/-}$ Dlk$^+$ cells. The screening of more than 39,000 transcripts successfully identified 75 down-regulated and 97 up-regulated genes (Supporting Table 1). As expected, enforced expression of *Bmi1* contributed to the maintenance of stemness features and suppression of differentiation-related genes. The present analysis revealed gene expression to be up-regulated for the hepatic stem cell markers *Prom1* (*CD133*) (P = 0.041) and *EpCAM* (P = 0.017) and down-regulated for the hepatocyte differentiation markers *Cps1* (P = 0.010), Mat1a (P = 0.011), and *Gjb2* (*Cx26*) (P = 0.010).

Among these, *Mat1a* knockout mice have been reported to be hypersensitive to oxidative stress and developed steatosis and HCC.[30] Furthermore, reduced expression of *Gjb2* (*Cx26*) is known to contribute to the promotion and progression of hepatocarcinogenesis in rats.[31]

Of interest, our microarray analysis unveiled the altered expression of genes involved in Wnt/β-catenin signaling; down-regulation of the Wnt antagonist *Sox17* ($P = 0.009$), up-regulation of a Wnt downstream effector *Cyclin D1* ($P = 0.001$), and modestly increased expression of the Wnt receptor *Fzd7* ($P = 0.098$). Wnt/β-catenin signaling is integrally associated with the regulation of stem cells and development of cancer[32] and activated Wnt/β-catenin signaling promotes the proliferation and transformation of hepatic stem/progenitor cells.[3] Together, these results imply that enforced expression of *Bmi1* results in an enhancement of stemness features and the acquisition of malignant potential in normal hepatic stem/progenitor cells, at least in part, through the activation of Wnt signaling. However, further analysis would be necessary to elucidate the relationship between Bmi1 and Wnt signaling.

Surprisingly but importantly, none of the 75 down-regulated genes following *Bmi1*-overexpression was included among the 305 up-regulated genes in neural progenitor cells after *Bmi1* knockdown.[27] Likewise, there existed no overlapping genes between the current expression profile and the 101 commonly regulated genes following *BMI1* knockdown between medulloblastoma and Ewing sarcoma cells.[33,34] In contrast, we detected several genes down-regulated following *Bmi1*-overexpression in hepatic stem/progenitor cells which are also regulated by Bmi1 in hematopoietic stem/progenitor cells (data not shown). These findings support the fact that PcG proteins function in a cell type-specific manner and the composition of PcG complexes is highly dynamic and differs in different cell-types and even at different gene loci.[35]

A comparison of the down-regulated genes with the ChIP-on-chip data for PcG complexes in ESCs revealed five genes that are regulated by PRC1 in ESCs as potential direct targets of Bmi1 in hepatic stem/progenitor cells (Fig. 6B). One of these genes, *Sox17*, is an endodermal marker gene and *Sox17*$^{-/-}$ mice die in the embryonic stage because the endoderm fails to form properly.[22] Therefore, its role in hepatic stem cells remained obscure. In the present study, self-renewal capacity of hepatic stem cells was inversely correlated with the *Sox17* expression levels. Furthermore, cotransduction of *Sox17* with *Bmi1* repressed tumorigenic capacity of Bmi1 in NOD/SCID mice. These findings suggest that Sox17 acts as a tumor suppressor in a specific type of tumor originating from hepatic stem cells. The finding that it is transcriptionally silenced by DNA methylation in human colon cancer cells further supports its role as a tumor suppressor gene.[36] On the other hand, *Sox17*-knockdown in Dlk^{+} cells alone did not promote tumor initiation in immunodeficient mice. Tumor initiation usually requires multiple steps including activation of oncogenes and repression of tumor suppressor genes. As a number of candidate genes of Bmi1 were identified in this study, coordinated regulation of multiple Bmi1 targets might be needed to recapitulate Bmi1-mediated tumorigenesis *in vivo*. In this regard, knockdown of *Sox17* or other candidate target genes in *Ink4a/Arf*$^{-/-}$ Dlk^{+} cells would be intriguing to assess for their tumorigenic activity *in vivo*.

Finally, our findings demonstrated that Bmi1 regulates the self-renewal of hepatic stem/progenitor cells to a large extent through the suppression of *Ink4a/Arf*. However, it is evident that targets of Bmi1 other than the *Ink4a/Arf* locus are also responsible for the development of cancer. Further analyses are necessary to determine the roles of the genes listed here in liver development, regeneration, and cancer.

Acknowledgment: The authors thank Dr. M. van Lohuizen for *Bmi1*$^{+/-}$ mice, Dr. W. Pear for the MIGR1 vector, Dr. Valentina M. Factor for the anti-A6 antibody, Dr. N. Nozaki for the anti-Bmi1 antibody, Dr. A. Miyawaki for Kusabira orange, Y. Yamazaki for technical support with the flow cytometry, and M. Tanemura for laboratory assistance.

References

1. Valk-Lingbeek ME, Bruggeman SWM, van Lohuizen M. Stem cells and cancer: the polycomb connection. Cell 2004;118:409-418.
2. Sparmann A, van Lohuizen M. Polycomb silencers control cell fate, development and cancer. Nat Rev Cancer 2006;6:846-856.
3. Chiba T, Zheng YW, Kita K, Yokosuka O, Saisho H, Onodera M, et al. Enhanced self-renewal capability in hepatic stem/progenitor cells drives cancer initiation. Gastroenterology 2007;133:937-950.
4. Mishra L, Banker T, Murray J, Byers S, Thenappan A, He AR, et al. Liver stem cells and hepatocellular carcinoma. HEPATOLOGY 2009;49: 318-329.
5. Lessard J, Sauvageau G. Bmi-1 determines the proliferative capacity of normal and leukaemic stem cells. Nature 2003;423:255-260.
6. Leung C, Lingbeek M, Shakhova O, Liu J, Tanger E, Saremaslani P, et al. Bmi1 is essential for cerebellar development and is overexpressed in human medulloblastomas. Nature 2004;428:337-341.
7. Pardal R, Clarke MF, Morrison SJ. Applying the principles of stem-cell biology to cancer. Nat Rev Cancer 2003;3:895-902.
8. Jamieson CH, Weissman IL, Passegue E. Chronic versus acute myelogenous leukemia: a question of self-renewal. Cancer Cell 2004;6:531-533.

9. Park IK, Morrison SJ, Clarke MF. Bmi1, stem cells, and senescence regulation. J Clin Invest 2004;113:175-179.
10. Iwama A, Oguro H, Negishi M, Kato Y, Morita Y, Tsukui H, et al. Enhanced self-renewal of hematopoietic stem cells mediated by the polycomb gene product Bmi-1. Immunity 2004;21:843-851.
11. Oguro H, Iwama A, Morita Y, Kamijo T, van Lohuizen M, Nakauchi H. Differential impact of Ink4a and Arf on hematopoietic stem cells and their bone marrow microenvironment in Bmi1-deficient mice. J Exp Med 2006;203:2247-2253.
12. Molofsky AV, He S, Bydon M, Morrison SJ, Pardal R. Bmi-1 promotes neural stem cell self-renewal and neural development but not mouse growth and survival by repressing the p16Ink4a and p19Arf senescence pathways. Genes Dev 2005;19:1432-1437.
13. Sasaki M, Ikeda H, Itatsu K, Yamaguchi J, Sawada S, Minato H, et al. The overexpression of polycomb group proteins Bmi1 and EZH2 is associated with the progression and aggressive biological behavior of hepatocellular carcinoma. Lab Invest 2008;88:873-882.
14. Tannapfel A, Busse C, Weinans L, Benicke M, Katalinic A, Geissler F, et al. INK4a-ARF alterations and p53 mutations in hepatocellular carcinomas. Oncogene 2001;20:7104-7109.
15. van der Lugt NM, Domen J, Linders K, van Roon M, Robanus-Maandag E, te Riele H, et al. Posterior transformation, neurological abnormalities, and severe hematopoietic defects in mice with a targeted deletion of the bmi-1 proto-oncogene. Genes Dev 1994;8:757-769.
16. Oertel M, Menthena A, Dabeva MD, Shafritz DA. Cell competition leads to a high level of normal liver reconstitution by transplanted fetal liver stem/progenitor cells. Gastroenterology 2006;130:507-520.
17. Dabeva MD, Petkov PM, Sandhu J, Oren R, Laconi E, Hurston E, et al. Proliferation and differentiation of fetal liver epithelial progenitor cells after transplantation into adult rat liver. Am J Pathol 2000;156:2017-2031.
18. Wang X, Foster M, Al-Dhalimy M, Lagasse E, Finegold M, Grompe M. The origin and liver repopulating capacity of murine oval cells. Proc Natl Acad Sci U S A 2003;100(Suppl. 1):11881-11888.
19. Boyer LA, Plath K, Zeitlinger J, Brambrink T, Medeiros LA, Lee TI, et al. Polycomb complexes repress developmental regulators in murine embryonic stem cells. Nature 2006;441:349-353.
20. Lee TI, Jenner RG, Boyer LA, Guenther MG, Levine SS, Kumar RM, et al. Control of developmental regulators by Polycomb in human embryonic stem cells. Cell 2006;125:301-313.
21. Bernstein BE, Mikkelsen TS, Xie X, Kamal M, Huebert DJ, Cuff J, et al. A bivalent chromatin structure marks key developmental genes in embryonic stem cells. Cell 2006;125:315-326.
22. Kanai-Azuma M, Kanai Y, Gad JM, Tajima Y, Taya C, Kurohmaru M, et al. Depletion of definitive gut endoderm in Sox17-null mutant mice. Development 2002;129:2367-2379.
23. Cho CH, Parashurama N, Park EY, Suganuma K, Nahmias Y, Park J, et al. Homogeneous differentiation of hepatocyte-like cells from embryonic stem cells: applications for the treatment of liver failure. FASEB J 2008;22:898-909.
24. Gil J, Peters G. Regulation of the INK4b-ARF-INK4a tumour suppressor locus: all for one or one for all. Nat Rev Mol Cell Biol 2006;7:667-677.
25. Akasaka T, van Lohuizen M, van der Lugt N, Mizutani-Koseki Y, Kanno M, Taniguchi M, et al. Mice doubly deficient for the Polycomb Group genes Mel18 and Bmi1 reveal synergy and requirement for maintenance but not initiation of Hox gene expression. Development 2001;128:1587-1597.
26. Dovey JS, Zacharek SJ, Kim CF, Lees JA. Bmi1 is critical for lung tumorigenesis and bronchioalveolar stem cell expansion. Proc Natl Acad Sci U S A 2008;105:11857-11862.
27. Fasano CA, Dimos JT, Ivanova NB, Lowry N, Lemischka IR, Temple S. shRNA knockdown of Bmi-1 reveals a critical role for p21-Rb pathway in NSC self-renewal during development. Cell Stem Cell 2007;1:87-99.
28. Bruggeman SW, Hulsman D, Tanger E, Buckle T, Blom M, Zevenhoven J, et al. Bmi1 controls tumor development in an Ink4a/Arf-independent manner in a mouse model for glioma. Cancer Cell 2007;12:328-341.
29. Serrano M, Lee H, Chin L, Cordon-Cardo C, Beach D, DePinho RA. Role of the *INK4a* locus in tumor suppression and cell mortality. Cell 1996;85:27-37.
30. Lu SC, Alvarez L, Huang ZZ, Chen L, An W, Corrales FJ, et al. Methionine adenosyltransferase 1A knockout mice are predisposed to liver injury and exhibit increased expression of genes involved in proliferation. Proc Natl Acad Sci U S A 2001;98:5560-5565.
31. Sakamoto H, Oyamada M, Enomoto K, Mori M. Differential changes in expression of gap junction proteins connexin 26 and 32 during hepatocarcinogenesis in rats. Jpn J Cancer Res 1992;83:1210-1215.
32. Reya T, Clevers H. Wnt singnaling in stem cells and cancer. Nature 2005;434:843-850.
33. Wiederschain D, Chen L, Johnson B, Bettano K, Jackson D, Taraszka J, et al. Contribution of polycomb homologues Bmi-1 and Mel-18 to medulloblastoma pathogenesis. Mol Cell Biol 2007;27:4968-4979.
34. Douglas D, Hsu JH, Hung L, Cooper A, Abdueva D, van Doorninck J, et al. BMI-1 promotes ewing sarcoma tumorigenicity independent of CDKN2A repression. Cancer Res 2008;68:6507-6515.
35. Orland V. Polycomb, epigenomes, and control of cell identity. Cell 2003;112:599-606.
36. Zhang W, Glöckner SC, Guo M, Machida EO, Wang DH, Easwaran H, et al. Epigenetic inactivation of the canonical Wnt antagonist SRY-box containing gene 17 in colorectal cancer. Cancer Res 2008;68:2764-2772.

Radiotherapy and Oncology 96 (2010) 231–235

Contents lists available at ScienceDirect

Radiotherapy and Oncology

journal homepage: www.thegreenjournal.com

Particle beam radiotherapy

Comparison of efficacy and toxicity of short-course carbon ion radiotherapy for hepatocellular carcinoma depending on their proximity to the porta hepatis

Hiroshi Imada [a,b,*], Hirotoshi Kato [a], Shigeo Yasuda [a], Shigeru Yamada [a], Takeshi Yanagi [a], Riwa Kishimoto [a], Susumu Kandatsu [a], Jun-etsu Mizoe [a], Tadashi Kamada [a], Osamu Yokosuka [b], Hirohiko Tsujii [a]

[a] *National Institute of Radiological Sciences, Chiba, Japan;* [b] *Department of Medicine and Clinical Oncology, Chiba University, Japan*

ARTICLE INFO

Article history:
Received 27 April 2009
Received in revised form 4 March 2010
Accepted 21 May 2010
Available online 25 June 2010

Keywords:
Radiotherapy
Carbon ion
Hepatocellular carcinoma
Porta hepatis

ABSTRACT

Background and purpose: To compare the efficacy and toxicity of short-course carbon ion radiotherapy (C-ion RT) for patients with hepatocellular carcinoma (HCC) in terms of tumor location: adjacent to the porta hepatis or not.

Materials and methods: The study consisted of 64 patients undergoing C-ion RT of 52.8 GyE in four fractions between April 2000 and March 2003. Of these patients, 18 had HCC located within 2 cm of the main portal vein (porta hepatis group) and 46 patients had HCC far from the porta hepatis (non-porta hepatis group). We compared local control, survival, and adverse events between the two groups.

Results: The 5-year overall survival and local control rates were 22.2% and 87.8% in the porta hepatis group and 34.8% and 95.7% in the non-porta hepatis group, respectively. There were no significant differences (P = 0.252, P = 0.306, respectively). Further, there were no significant differences in toxicities. Biliary stricture associated with C-ion RT did not occur.

Conclusions: Excellent local control was obtained independent of tumor location. The short-course C-ion RT of 52.8 GyE in four fractions appears to be an effective and safe treatment modality in the porta hepatis group just as in the non-porta hepatis group.

Hepatocellular carcinoma (HCC) is one of the most common malignant tumors worldwide and is the third leading cause of death from cancer [1]. Various therapeutic options are presently available for patients with HCC. In radiotherapy, the role for patients with HCC was previously limited and unsatisfactory on the basis of its poor hepatic tolerance to irradiation [2,3]. Technological advances have made it possible to deliver a higher dose of radiation to focal liver tumors accurately, reducing the degree of toxicity [4–7]. Proton beam therapy was shown to be effective and safe for HCC, mainly due to its excellent dose distribution at the end of the beam path, called the Bragg peak [8–10]. Carbon ion beams also possess the Bragg peak, and they provide excellent dose distribution to the target volume by specified beam modulations [11–15]. They have advantageous biological and physical properties that result in a higher cytocidal effect than that of photons and protons [16–19]. Since 1995, carbon ion radiotherapy (C-ion RT) has been performed for treatment of HCC, and clinical trials were initiated at the National Institute of Radiological Sciences (NIRS).

In terms of HCC adjacent to the porta hepatis, treatment with minimal invasiveness and complications is an important issue. Surgical resection is the standard of curative treatment, but it is restricted to selected patients due to degradation of hepatic function [20,21]. Liver transplantation is a curative treatment of HCC, but it is often not feasible [22–24] and a shortage of donors also limits its possibilities. Radiofrequency ablation (RFA) and other ablative techniques obtain excellent local control, but are limited largely to small HCCs [25–27]. In the presence of blood vessels contiguous with tumor, blood flow reduces the thermal effects of RFA [28–30]. In addition, biliary complications after RFA for HCC adjacent to the porta hepatis sometimes occur, resulting in septic complications and liver failure [31].

We have already reported that C-ion RT used for the treatment of HCC is safe and effective [17,19]. In this study, patients were stratified into two groups according to tumor localization: adjacent to the porta hepatis or not. We compared the treatment effect and toxicity between the two groups retrospectively.

Materials and methods

Patients

Between April 2000 and March 2003, 64 patients with HCC underwent 52.8 GyE/4-fraction C-ion RT in a phase I/II clinical trial or phase II clinical trial at NIRS. The phase I/II clinical trial was carried out from April 2000 to March 2001, and the phase II clinical

* Corresponding author. Address: Research Center for Charged Particle Therapy, National Institute of Radiological Sciences, 4-9-1, Anagawa, Inage-ku, Chiba 263-8555, Japan.
E-mail address: h_imada@nirs.go.jp (H. Imada).

0167-8140/$ - see front matter © 2010 Elsevier Ireland Ltd. All rights reserved.
doi:10.1016/j.radonc.2010.05.019

Table 1
Patient and tumor characteristics.

	Total	Porta hepatis group	Non-porta hepatis group	*P*
N	64	18	46	
Gender, *n* (%)				>0.999
Male	48 (75)	14 (78)	34 (74)	
Female	16 (25)	4 (22)	12 (26)	
Age (years)				0.736
Median	69	68	69	
Range	37–84	51–79	37–84	
Child-Pugh classification, *n* (%)				0.198
A	49 (77)	16 (89)	33 (72)	
B	15 (23)	2 (11)	13 (28)	
Stage (UICC 5th), *n* (%)				0.438
II	23 (36)	5 (28)	18 (39)	
IIIA	32 (50)	9 (50)	23 (50)	
IVA	9 (14)	4 (22)	5 (11)	
Maximum tumor diameter (mm)				0.725
Median	40.0	36.5	40.0	
Range	12–120	21–120	12–112	
Vascular invasion				0.066
Yes	45 (70)	16 (89)	29 (63)	
No	19 (30)	2 (11)	17 (37)	
Number of tumors, *n* (%)				0.676
Single	56 (88)	15 (83)	41 (89)	
Multiple	8 (12)	3 (17)	5 (11)	

Abbreviations: UICC = International Union against cancer.

trial was sequentially performed from April 2001 to March 2003. The eligibility criteria were previously reported [17]. HCC was diagnosed by needle biopsy in all patients. Prior to treatment, all patients gave their informed consent in writing in accordance with the Declaration of Helsinki. These clinical trials were approved by the ethics committees at NIRS. Eighteen of the 64 patients had HCC located within 2 cm from the main portal vein, and the other 46 had HCC far from the porta hepatis.

Background data of the patients and tumors are presented in Table 1. The enrolled patients consisted of 48 males and 16 females. Median age was 69 years (range, 37–84). Child-Pugh classification of the degree of liver impairment was as follows: 49 patients were categorized as Class A (scores, 5–6), and 15 patients as Class B (scores, 7–9). Twenty-three patients had Stage II, 32 had Stage IIIA, and 9 had Stage IVA. By the Barcelona Clinic Liver Cancer staging classification [32,33], 2 patients had Stage A and 16 had Stage C in the porta hepatis group, and 15 had Stage A, 2 had Stage B, and 29 had Stage C in the non-porta hepatis group. Median maximum tumor diameter was 40 mm (range, 12–120). Forty-five patients had vascular invasion. Fifty-six patients had a solitary mass and 8 had multiple tumors.

Pretreatment evaluation

Laboratory values collected for all patients included complete blood cell counts, liver and renal function tests, electrolytes, HBV and HCV titers, and α-fetoprotein (AFP). Abdominal triphasic CT or MRI was performed for evaluation of the extent of HCC.

C-ion RT

The carbon ion beam used for radiotherapy was generated by the heavy ion medical accelerator in Chiba developed by NIRS in 1993. The accelerator system and the biophysical characteristics of the carbon ion beam have been previously described [13–15]. For modulation of the Bragg peak of the beam to conform to the target volume, the beam lines in the treatment room are equipped with a pair of wobbler magnets, beam scatterers, ridge filters, multileaf collimators, and a compensation bolus.

Before therapeutic planning, all patients had metallic markers (iridium seeds, 0.5 mm in diameter and 3 mm in length) implanted near the tumor to obtain precise treatment positioning. The irradiation fields were established with a three-dimensional therapy plan on the basis of 5-mm-thick CT images. The planning target volume was defined according to the shape of the tumor plus a 1.0–1.2 cm margin. To reproduce the target position accurately, a low-temperature thermoplastic sheet (Shellfitter, Kuraray, Osaka, Japan), a customized cradle (Moldcare, Alcare, Tokyo, Japan), and a respiratory gated irradiation system [34] were used in the CT planning and radiotherapy performance. The radiation field was confirmed and corrected by orthogonal fluoroscopy and radiography immediately before each treatment session.

Irradiation doses were expressed in Gray equivalents (GyE = carbon physical dose [in Gray] × relative biologic effectiveness). The relative biologic effectiveness value of carbon ions was assumed to be 3 at the distal part of the spread-out Bragg peak [35]. C-ion RT was given once daily, 4 days a week, for four fractions in 1 week. The dose per fraction was 13.2 GyE, so all patients received a total dose of 52.8 GyE.

Follow-up and evaluation criteria

All patients were assessed according to a predetermined schedule. After C-ion RT, patients were evaluated on the basis of physical examinations and blood tests once a month for the first year, once every 3 months for the following year, and once every 3–6 months thereafter. Contrast-enhanced CT or MRI was performed every 3 months for the first 2 years and every 6 months thereafter. Local control was defined as no sign of regrowth or new tumor in the treatment volume. Local recurrence was defined as failure of local control. Overall survival was measured from the starting date of treatment until the date of death from any cause. Cause-specific survival was defined as the interval between the starting date of treatment and the date of death from liver failure or HCC. Disease-free survival was defined as the interval between the starting date of treatment and the date of the diagnosis of the first recurrence or death from any cause. Acute and late toxicities were assessed using the National Cancer Institute Common Criteria, version 2.0, and the Radiation Therapy Oncology Group/European Organization for Research and Treatment of Cancer late radiation morbidity scoring scheme. Liver toxicity in late phase was assessed by Child-Pugh score, a commonly used marker of hepatic functional reserve in chronic liver disease.

Statistical analysis

Statistical analyses were performed using SPSS version 12.0 (SPSS Inc., Chicago, IL). For continuous variables, non-parametric tests (Mann–Whitney *U* test) were used. For categorical data, chi-squared test or Fisher's exact test was used. The Kaplan–Meier method was used for calculation of local control and survival rates, and the survival curves were compared by log-rank test. Statistical significance was considered if $P < 0.05$ (*P*-values from two-sided tests).

Results

There were no significant differences in sex, age, Child-Pugh classification, clinical stage, maximum tumor diameter, and tumor number between the two groups. The porta hepatis group exhibited greater vascular invasion than the non-porta hepatis group ($P = 0.066$).

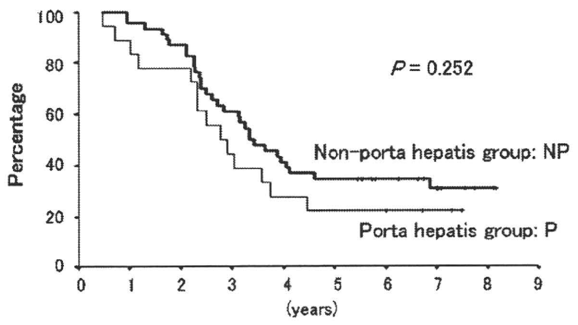

Number of patients at risk

NP	46	44	40	28	19	16	12	7	2	0
P	18	16	14	8	5	4	4	2	0	0

Fig. 1. Overall survival rate according to tumor localization. Overall survival rates after 3 and 5 years were 44.4% and 22.2% in the porta hepatis group and 60.9% and 34.8% in the non-porta hepatis group, respectively. There were no significant differences between the two groups ($P = 0.252$).

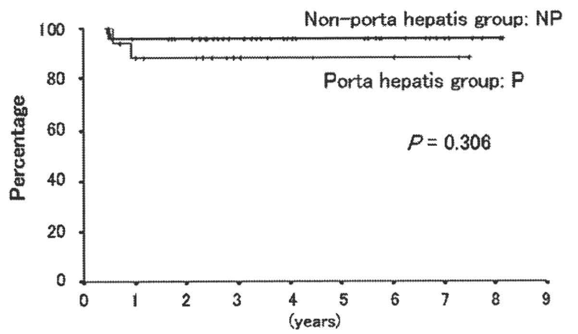

Number of patients at risk

NP	46	42	39	28	19	16	12	7	2	0
P	18	14	12	6	4	3	3	2	0	0

Fig. 2. Local control rate according to tumor localization. Local control rates after both 3 and 5 years were 87.8% in the porta hepatis group and 95.7% in the non-porta hepatis group. There were no significant differences between the two groups ($P = 0.306$).

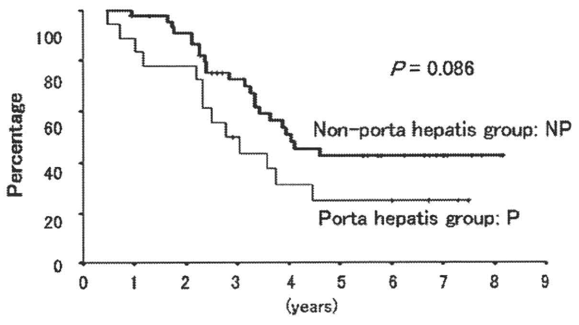

Number of patients at risk

NP	46	44	40	28	19	16	12	7	2	0
P	18	16	14	8	5	4	4	2	0	0

Fig. 3. Cause-specific survival rate according to tumor localization. Cause-specific survival rates after 3 and 5 years were 50.0% and 25.0% in the porta hepatis group and 72.3% and 42.8% in the non-porta hepatis group, respectively. The porta hepatis group showed a trend towards inferior outcome compared to the non-porta hepatis group ($P = 0.086$).

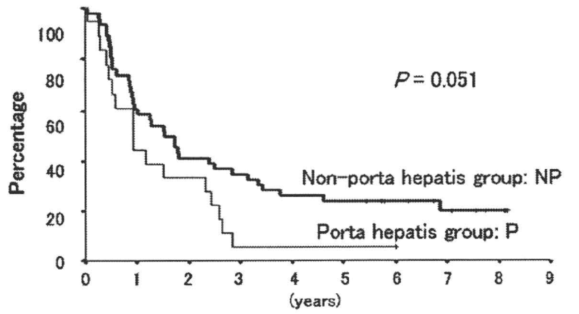

Number of patients at risk

NP	46	28	19	16	12	11	8	5	2	0
P	18	8	6	1	1	1	1	0	0	0

Fig. 4. Disease-free survival rate according to tumor localization. Disease-free survival rates after both 3 and 5 years were 5.6% in the porta hepatis group, and they were 34.8% and 23.9% in the non-porta hepatis group, respectively. The porta hepatis group showed a trend towards inferior outcome compared to the non-porta hepatis group ($P = 0.051$).

The median observation period for survival was 34 months (range, 6–90 months) in the porta hepatis group and 41 months (range, 11–98 months) in the non-porta hepatis group. Four patients were alive at last follow-up and 14 had died in the porta hepatis group, and 15 were alive at last follow-up and 31 had died in the non-porta hepatis group. Overall survival rates after 3 and 5 years were 44.4% [95% confidence interval (CI), 22–67] and 22.2% [95% CI, 3–41] in the porta hepatis group and 60.9% [95% CI, 47–75] and 34.8% [95% CI, 21–49] in the non-porta hepatis group, respectively (Fig. 1). Local control rates after both 3 and 5 years were 87.8% [95% CI, 72–104] in the porta hepatis group and 95.7% [95% CI, 90–102] in the non-porta hepatis group, respectively (Fig. 2). There were no significant differences between the two groups in overall survival and local control rates ($P = 0.252$, $P = 0.306$, respectively). Cause-specific survival rates after 3 and 5 years were 50.0% [95% CI, 27–73] and 25.0% [95% CI, 4–46] in the porta hepatis group and 72.3% [95% CI, 59–86] and 42.8% [95% CI, 27–58] in the non-porta hepatis group, respectively (Fig. 3). Disease-free survival rates after both 3 and 5 years were 5.6% [95% CI, −5 to 16] in the porta hepatis group, and they were 34.8% [95% CI, 21–49] and 23.9% [95% CI, 12–36] in the non-porta hepatis group, respectively (Fig. 4). In the cause-specific and disease-free survival rates, the porta hepatis group showed a trend towards inferior outcome compared to the non-porta hepatis group ($P = 0.086$, $P = 0.051$, respectively).

Toxicities in early phase are shown in Table 2. Adverse events of grade 3 or more were compared between the two groups. There were no significant differences in hepatic and hematologic toxicities ($P > 0.999$, $P = 0.190$, respectively). As to Child-Pugh score in late phase, cases with changes in Child-Pugh score within 1-point increase were 13 in the porta hepatis group and 41 in the non-porta hepatis group. Those with changes in score increasing by at least 2 points were five in each of the groups. There were no significant differences between the two groups in terms of change in Child-Pugh score (≦1 vs. ≧2) ($P = 0.128$) (Table 3). In terms of other non-hematologic toxicities such as skin and gastrointestinal toxicities, toxicities of grade 3 or higher did not occur. No patient had biliary stenosis associated with C-ion RT.

Table 2
Toxicities in early phase.

	Porta hepatis group Grade					Non-porta hepatis group Grade				
	0	1	2	3	4	0	1	2	3	4
Liver	2	4	9	3	0	7	15	16	8	0
Blood	6	2	4	6	0	13	9	16	8	0

There were no significant differences between porta hepatis and non-porta hepatis groups in liver and blood toxicities (grade 0–2 vs. grade 3–4) by Fisher's exact test. $P > 0.999$ (liver toxicity); $P = 0.190$ (blood toxicity).

Table 3
Change of Child-Pugh score in late phase.

	≦1	≧2
Porta hepatis group	13	5
Non-porta hepatis group	41	5

There were no significant differences between porta hepatis and non-porta hepatis groups in change of Child-Pugh score (≦1 vs. ≧2) by Fisher's exact test. $P = 0.128$.

Discussion

It is important that the treatment of HCC involves minimum invasiveness and complications in general. Surgical resection and RFA are essential curative therapies for HCC. In surgical resection, it was reported that both the 5-year overall survival and disease-free survival rates of the anatomic resection group were significantly better than those of the non-anatomic resection group, as HCC has a nature to cause intrahepatic metastasis via vascular invasion [36]. Anatomic resection consists of the systematic removal of a hepatic segment confined by tumor-bearing portal tributaries. In some patients with HCC adjacent to the porta hepatis, anatomic resection implies greater invasiveness because the resection volume becomes larger.

Concerning the use of RFA, puncture of the liver hilus, with the risk of injury to the portal vein or bile duct, presents a potentially dangerous scenario. It was reported that RFA was performed for patients with HCC adjacent to the porta hepatis under the condition of cooling the bile duct by endoscopic nasobiliary drainage tube to prevent biliary complications [31]. But the procedure is too complex to be a common therapy. Additionally, in cases of HCC with contiguous vessels, blood flow reduces the thermal effects of RFA, a phenomenon that increases the likelihood of the presence of residual viable tumor cells [37–39].

According to the above, we need to consider the degree of invasiveness and complications and carefully select an appropriate treatment modality because HCC adjacent to the porta hepatis is close to vessels and bile duct. In this study, therefore, differences in treatment effect and toxicities according to tumor localization, whether adjacent to the porta hepatis or not, were investigated retrospectively.

In the comparison of patient and tumor characteristics, the porta hepatis group demonstrated a trend towards a higher rate of vascular invasion compared to the non-porta hepatis group ($P = 0.066$). It is suggested that this was due to the tumor location.

Local control rates after 5 years were 87.8% [95% CI, 72–104] in the porta hepatis group and 95.7% [95% CI, 90–102] in the non-porta hepatis group. Thus, we obtained excellent local control rates in both groups. Local failure occurred in only four of all patients—two each in the porta hepatis and non-porta hepatis groups. There were no significant differences in toxicities. Biliary stenosis associated with C-ion RT did not occur in either group. Therefore, in certain patients with a higher risk of injury to the bile duct when undergoing RFA, in high-risk cases such as elderly patients for postoperative complications after surgical resection, or in some patients who refuse to undergo hepatectomy or RFA, C-ion RT appears to offer a promising therapeutic alternative for HCC.

However, cause-specific and disease-free survival rates after 5 years were 25.0% [95% CI, 4–46] and 5.6% [95% CI, −5 to 16] in the porta hepatis group and 42.8% [95% CI, 27–58] and 23.9% [95% CI, 12–36] in the non-porta hepatis group, respectively, which indicates a difference which is of borderline significance ($P = 0.086$, $P = 0.051$). The presence of vascular invasion is higher in the porta hepatis group ($P = 0.066$). A characteristic of HCC is the potential of causing intrahepatic metastasis via vascular invasion, and therefore the cause-specific and disease-free survival rates are mainly representing the rate of intrahepatic metastases/new tumors as there were almost no local failures (Fig. 2). This emphasizes the necessity to take into account the possibility of intrahepatic metastasis via vascular invasion. Of course, the importance of the earliest possible detection of a new tumor lesion and its treatment with an appropriate therapeutic modality cannot be overstated. In this regard, it is considered especially important to keep in mind the clinical multidisciplinary approach available for treating HCC.

As for radiation therapy for HCC adjacent to the porta hepatis, it was reported that proton beam therapy delivering 72.6 GyE in 22 fractions appears effective and safe. Overall 3-year survival and local control rates were 45.1% and 86.0%, respectively [40]. In our study, these rates in the porta hepatis group were 44.4% [95% CI, 22–67] and 87.8% [95% CI, 72–104], respectively. Therefore, the treatment effect of short-course C-ion RT is suggested to be almost equal to that of proton beam therapy with a more fractionated regimen.

A limitation of this study was the fact that the patient number in the porta hepatis group was small. It is therefore important to collect such cases and continuously verify efficacy and safety of short-course C-ion RT for patients with HCC adjacent to the porta hepatis.

In conclusion, excellent local control was achieved independent of tumor localization. There was no significant difference in treatment-related toxicity between the porta hepatis and non-porta hepatis groups. The short-course C-ion RT of 52.8 GyE in four fractions appears to be an effective and safe therapeutic option for porta hepatis patients just as it is for non-porta hepatis patients.

Conflict of interest statement

Any actual or potential conflicts of interest do not exist.

Acknowledgements

This study was supported by the Research Project with Heavy Ions of the National Institute of Radiological Sciences in Japan. We are grateful to the members of the National Institute of Radiological Sciences.

References

[1] Bosch FX, Ribes J, Borras J. Epidemiology of primary liver cancer. Semin Liver Dis 1999;19:271–85.
[2] Phillips R, Murakami K. Preliminary neoplasms of the liver. Results of radiation therapy. Cancer 1960;13:714–20.
[3] Stillwagon GB, Order SE, Guse C, et al. 194 Hepatocellular cancers treated by radiation and chemotherapy combinations: Toxicity and response: a Radiation Therapy Oncology Group study. Int J Radiat Oncol Biol Phys 1989;17:1223–9.
[4] Robertson JM, Lawrence TS, Dworzanin LM, et al. Treatment of primary hepatobiliary cancers with conformal radiation therapy and regional chemotherapy. J Clin Oncol 1993;11:1286–93.
[5] Toya R, Murakami R, Baba Y, et al. Conformal radiation therapy for portal vein tumor thrombosis of hepatocellular carcinoma. Radiother Oncol 2007;84:266–71.

[6] Xi M, Liu MZ, Deng XW, et al. Defining internal target volume (ITV) for hepatocellular carcinoma using four-dimensional CT. Radiother Oncol 2007;84:272–8.
[7] Zhao JD, Xu ZY, Zhu J, et al. Application of active breathing control in 3-dimensional conformal radiation therapy for hepatocellular carcinoma: the feasibility and benefit. Radiother Oncol 2008;87:439–44.
[8] Suit HD, Goitein M, Munzenrider J, et al. Increased efficacy of radiation therapy by use of proton beam. Strahlenther Onkol 1990;166:40–4.
[9] Matsuzaki Y, Osuga T, Saito Y, et al. A new, effective, and safe therapeutic option using proton irradiation for hepatocellular carcinoma. Gastroenterology 1994;106:1032–41.
[10] Matsuzaki Y. The efficacy of powerful proton radiotherapy for hepatocellular carcinoma-long term effects and QOL. Ann Cancer Res Ther 1998;7:9–17.
[11] Blakely EA, Ngo FQH, Curtis SB, et al. Heavy ion radiobiology: cellular studies. Adv Radiat Biol 1984;11:295–378.
[12] Castro JR. Future research strategy for heavy ion radiotherapy. In: Kogelnih HD, editor. Progress in radio-oncology. Bologna: Monduzzi Editore; 1995. p. 643–8.
[13] Sato K, Yamada H, Ogawa K, et al. Performance of HIMAC. Nucl Phys 1995;A588:229–34.
[14] Kanai T, Furusawa Y, Fukutsu K, Itsukaichi H, Eguchi-Kasai K, Ohara H. Irradiation of mixed beam and design of spread-out Bragg peak for heavy-ion radiotherapy. Radiat Res 1997;147:78–85.
[15] Kanai T, Endo M, Minohara S, et al. Biophysical characteristics of HIMAC clinical irradiation system for heavy-ion radiation therapy. Int J Radiat Oncol Biol Phys 1999;44:201–10.
[16] Tsujii H, Morita S, Miyamoto T, et al. Preliminary results of phase I/II carbon ion therapy. J Brachyther Int 1997;13:1–8.
[17] Kato H, Tsujii H, Miyamoto T, et al. Results of the first prospective study of carbon ion radiotherapy for hepatocellular carcinoma with liver cirrhosis. Int J Radiat Oncol Biol Phys 2004;59:1468–76.
[18] Tsujii H, Mizoe JE, Kamada T, et al. Overview of clinical experiences on carbon ion radiotherapy at NIRS. Radiother Oncol 2004;73:S41–49.
[19] Kato H, Yamada S, Yasuda S, et al. Phase II study of short-course carbon ion radiotherapy (52.8 GyE/4-fraction/1-week) for hepatocellular carcinoma. Hepatology 2005;42:381A.
[20] Ikai I, Arii S, Okazaki M, et al. Report of the 17th nationwide follow-up survey of primary liver cancer in Japan. Hepatol Res 2007;37:676–91.
[21] Mulcahy MF. Management of hepatocellular cancer. Curr Treat Options Oncol 2005;6:423–35.
[22] Mazzaferro V, Regalia E, Doci R, et al. Liver transplantation for the treatment of small hepatocellular carcinomas in patients with cirrhosis. N Engl J Med 1996;334:693–9.
[23] Llovet JM, Fuster J, Bruix J. Intention-to-treat analysis of surgical treatment for early hepatocellular carcinoma: resection versus transplantation. Hepatology 1999;30:1434–40.
[24] Yoo HY, Patt CH, Geschwind JF, et al. The outcome of liver transplantation in patients with hepatocellular carcinoma in the United States between 1988 and 2001: 5-year survival has improved significantly with time. J Clin Oncol 2003;21:4329–35.
[25] Kuvshinoff BW, Ota DM. Radiofrequency ablation of liver tumors: influence of technique and tumor size. Surgery 2002;132:605–11.
[26] Shiina S, Teratani T, Obi S, et al. A randomized controlled trial of radiofrequency ablation with ethanol injection for small hepatocellular carcinoma. Gastroenterology 2005;129:122–30.
[27] Sato M, Watanabe Y, Ueda S, et al. Microwave coagulation therapy for hepatocellular carcinoma. Gastroenterology 1996;110:1507–14.
[28] Patterson EJ, Scudamore CH, Owen DA, et al. Radiofrequency ablation of porcine liver in vivo: effects of blood flow and treatment time on lesion size. Ann Surg 1998;227:559–65.
[29] Livraghi T, Solbiati L, Meloni MF, et al. Treatment of focal liver tumors with percutaneous radio-frequency ablation: complications encountered in a multicenter study. Radiology 2003;226:441–51.
[30] Nakazawa T, Kokubu S, Shibuya A, et al. Radiofrequency ablation of hepatocellular carcinoma: correlation between local tumor progression after ablation and ablative margin. AJR Am J Roentgenol 2007;188:480–8.
[31] Ohnishi T, Yasuda I, Nishigaki Y, et al. Intraductal chilled saline perfusion to prevent bile duct injury during percutaneous radiofrequency ablation for hepatocellular carcinoma. J Gastroenterol Hepatol 2008;23:e410–415.
[32] Llovet JM, Bru C, Bruix J. Prognosis of hepatocellular carcinoma: the BCLC staging classification. Semin liver Dis 1999;19:329–38.
[33] Llovet JM, Burroughs A, Bruix J. Hepatocellular carcinoma. Lancet 2003;362:1907–17.
[34] Minohara S, Kanai T, Endo M, Noda K, Kanazawa M. Respiratory gated irradiation system for heavy-ion radiotherapy. Int J Radiat Oncol Biol Phys 2000;47:1097–103.
[35] Suzuki M, Kase Y, Yamaguchi H, Kanai T, Ando K. Relative biological effectiveness for cell-killing effect on various human cell lines irradiated with heavy-ion medical accelerator in Chiba (HIMAC) carbon-ion beams. Int J Radiat Oncol Biol Phys 2000;48:241–50.
[36] Hasegawa K, Kokudo N, Imamura H, et al. Prognostic impact of anatomic resection for hepatocellular carcinoma. Ann Surg 2005;242:252–9.
[37] Rossi S, Garbagnati F, Lencioni R, et al. Percutaneous radio-frequency thermal ablation of nonresectable hepatocellular carcinoma after occlusion of tumor blood supply. Radiology 2000;217:119–26.
[38] McGhana JP, Dodd 3rd GD. Radiofrequency ablation of the liver: current status. AJR Am J Roentgenol 2001;176:3–16.
[39] de Baere T, Denys A, Wood BJ, et al. Radiofrequency liver ablation: experimental comparative study of water-cooled versus expandable systems. AJR Am J Roentgenol 2001;176:187–92.
[40] Mizumoto M, Tokuuye K, Sugahara S, et al. Proton beam therapy for hepatocellular carcinoma adjacent to the prota hepatis. Int J Radiat Oncol Biol Phys 2008;71:462–7.

Radiotherapy and Oncology 96 (2010) 236–242

Contents lists available at ScienceDirect

Radiotherapy and Oncology

journal homepage: www.thegreenjournal.com

Particle beam radiotherapy

Compensatory enlargement of the liver after treatment of hepatocellular carcinoma with carbon ion radiotherapy – Relation to prognosis and liver function

Hiroshi Imada [a,b,*], Hirotoshi Kato [a], Shigeo Yasuda [a], Shigeru Yamada [a], Takeshi Yanagi [a], Ryusuke Hara [a], Riwa Kishimoto [a], Susumu Kandatsu [a], Shinichi Minohara [a], Jun-etsu Mizoe [a], Tadashi Kamada [a], Osamu Yokosuka [b], Hirohiko Tsujii [a]

[a] *Research Center for Charged Particle Therapy, National Institute of Radiological Sciences, Chiba, Japan;* [b] *Department of Medicine and Clinical Oncology, Graduate School of Medicine, Chiba University, Chiba, Japan*

ARTICLE INFO

Article history:
Received 30 December 2008
Received in revised form 3 December 2009
Accepted 18 March 2010
Available online 21 April 2010

Keywords:
Hepatocellular carcinoma
Radiotherapy
Carbon ion
Liver volume
Liver function

ABSTRACT

Background and purpose: To examine whether liver volume changes affect prognosis and hepatic function in patients treated with carbon ion radiotherapy (CIRT) for hepatocellular carcinoma (HCC).

Material and methods: Between April 1995 and March 2003, among the cases treated with CIRT, 43 patients with HCC limited to the right hepatic lobe were considered eligible for the study. The left lateral segment was defined as the non-irradiated region. Liver volume was measured using contrast CT at 0, 3, 6, and 12 months after CIRT. We examined serum albumin, prothrombin activity, and total bilirubin level as hepatic functional reserve.

Results: After CIRT, the non-irradiated region showed significant enlargement, and enlarged volume of this region 3 months after CIRT $\geqslant 50$ cm^3 was a prognostic factor. The 5-year overall survival rates were 48.9% in the larger enlargement group (enlarged volume of non-irradiated region 3 months after CIRT $\geqslant 50$ cm^3) and 29.4% in the smaller enlargement group (as above, <50 cm^3). The larger enlargement group showed better hepatic functional reserve than the smaller enlargement group 12 months after CIRT.

Conclusions: This study suggests that compensatory enlargement in the non-irradiated liver after CIRT contributes to the improvement of prognosis.

Hepatocellular carcinoma (HCC) is one of the most common malignant tumors in the world and is the third-leading cause of death from cancer [1]. In Japan, its incidence is approximately 30 in 100,000 males and 10 in 100,000 females [2]. HCC is closely associated with hepatitis B and C, and the majority of patients with HCC have liver cirrhosis, a condition that limits treatment options. Surgical resection is the mainstay of curative treatment, but it is restricted to selected patients [3,4]. Radiofrequency ablation and other ablative techniques achieve excellent local control, but they are restricted to small HCC [5–7]. Transcatheter arterial chemoembolization is clinically useful [8–10], but a radical effect has not been proved in histopathologic studies [11,12]. There is an urgent need for more effective and less invasive treatment of HCC.

The previous role of radiotherapy for HCC was limited and unsatisfactory by poor hepatic tolerance to irradiation [13,14]. Technological advances have made it possible to deliver a higher dose of radiation to focal liver cancers accurately, reducing the risk of toxicity [15–17]. Proton beam therapy has appeared to be effective and safe for HCC, mainly because of its excellent dose distribution at the end of the beam path, called the Bragg peak [18,19]. Carbon ion beams also possess the Bragg peak, and they provide excellent dose localization to the target volume by specified beam modulations [20,21]. They have advantageous biological and physical properties that result in a higher cytocidal effect than those of photons and protons [22–27].

The history of the use of carbon ion radiotherapy (CIRT) for treating HCC goes back to 1995, when clinical trials were initiated at the National Institute of Radiological Sciences (NIRS). We have already reported that CIRT used for the treatment of HCC is safe and effective, and that it causes only minor liver damage [22,23]. Although atrophy of the irradiated region of the liver is observed after CIRT, the reason why liver function is retained after CIRT has not yet been investigated.

It has been reported that preoperative portal vein embolization in extended hepatectomy cases causes the remnant liver volume to increase and postoperative hepatic insufficiency to diminish [28,29]. Similarly, we wondered whether the same mechanism might apply to CIRT. Thus, as the region irradiated with CIRT showed atrophy and the non-irradiated region appeared to show

* Corresponding author at: Research Center for Charged Particle Therapy, National Institute of Radiological Sciences, 4-9-1, Anagawa, Inage-ku, Chiba 263-8555, Japan.
E-mail address: h_imada@nirs.go.jp (H. Imada).

0167-8140/$ - see front matter © 2010 Elsevier Ireland Ltd. All rights reserved.
doi:10.1016/j.radonc.2010.03.025

compensatory enlargement after CIRT, it was supposed that the compensatory enlargement had a contributory role in the retention of hepatic function. This hypothesis was investigated.

Materials and methods

Patients

CIRT for HCC was performed as a Phase I/II clinical trial from April 1995 through March 2001 with 110 patients, and as a Phase II clinical trial from April 2001 through March 2003 with 47 patients. The eligibility criteria for enrollment in these clinical trials were previously reported [22]. Prior to treatment, all patients gave their written informed consent in accordance with the Declaration of Helsinki. One hundred twenty-one of the total 157 had the tumor limited to the right lobe of the liver, 27 had the tumor limited to the left lobe, and 9 had the tumor in both right and left lobes.

Among the patients of this study, 43 met the following conditions: (1) treatment target tumor was limited to the right lobe of the liver, (2) left lateral segment was not irradiated, (3) no additional treatment was performed for hepatic lesions (local recurrence and/or recurrence in other loci) within 12 months after CIRT, and (4) abdominal contrast CT imaging was performed at our institute at 0, 3, 6 and 12 months after CIRT. Background data of the patients and tumors are presented in Table 1. The regions irradiated with more than 10% radiation dose were as follows: anterior, posterior and medial segments in 32 patients, anterior and posterior segments in 8, posterior segment in 2, and anterior and medial segments in 1.

Carbon ion radiotherapy

The carbon ion beam used for radiotherapy was generated from the heavy ion medical accelerator in Chiba developed by NIRS in 1993. The accelerator system and the biophysical characteristics of the carbon ion beam have been previously described [20,21,30]. For modulation of the Bragg peak of the beam to conform to the target volume, the beam lines in the treatment room are equipped with a pair of wobbler magnets, beam scatterers, ridge filters, multileaf collimators, and a compensation bolus. The irradiation fields were established with a three-dimensional therapy plan on the basis of 5-mm-thick CT images. The planning target volume was defined according to the shape of the tumor plus a 1.0–1.2 cm margin. To reproduce the target position accurately, a low-temperature thermoplastic sheet (Shellfitter, Kuraray, Osaka, Japan), a customized cradle (Moldcare, Alcare, Tokyo, Japan), and a respiratory gated irradiation system [31] were used in the CT planning and radiotherapy stages. The radiation field was confirmed and corrected by orthogonal fluoroscopy and radiography immediately before each treatment session.

Table 1
Patient and tumor characteristics.

	Total	Larger enlargement group	Smaller enlargement group	*P*
n	43	20	23	
Gender, n (%)				
Male	29 (67)	15 (75)	14 (61)	0.353
Female	14 (33)	5 (25)	9 (39)	
Age (years)				
Median	66	71.5	65	0.006
Range	45–83	46–81	45–83	
Child-Pugh classification, n (%)				
A	35 (81)	18 (90)	17 (74)	0.250
B	8 (19)	2 (10)	6 (26)	
Stage (UICC 5th), n (%)				
I	13 (32)	6 (27)	7 (36)	0.947
II	25 (54)	12 (59)	13 (50)	
IIIA	5 (14)	2 (14)	3 (14)	
Gross tumor volume (cm^3)				
Median	35.2	54.7	31.8	0.114
Range	4.6–861.9	15.6–861.9	4.6–211.2	
Planning target volume (cm^3)				
Median	190.5	242.9	149.0	0.019
Range	39.6–1466.4	70.3–1466.4	39.6–538	
Liver volume of irradiated site (cm^3), mean ± SD	756.6 ± 134.1	767.1 ± 138.1	747.5 ± 132.9	0.942
Liver volume of non-irradiated site (cm^3), mean ± SD	320.0 ± 166.3	317.2 ± 152.7	322.4 ± 180.6	0.715
Albumin (g/dl), mean ± SD	3.8 ± 0.4	3.9 ± 0.4	3.8 ± 0.4	0.659
Prothrombin activity (%), mean ± SD	77.2 ± 13.5	78.6 ± 11.4	76.0 ± 15.3	0.670
Total bilirubin (mg/dl), mean ± SD	1.0 ± 0.4	0.9 ± 0.3	1.1 ± 0.4	0.072
Platelet count ($\times 10^4/\mu l$), mean ± SD	11.8 ± 4.6	14.0 ± 4.3	9.9 ± 3.9	0.002
Number of tumors, n (%)				
1	36 (84)	19 (95)	17 (74)	0.100
2	7 (16)	1 (5)	6 (26)	
Irradiated segment, n (%)				
Anterior, posterior and medial	32	15	17	0.821
Anterior and posterior	8	4	4	
Posterior	2	1	1	
Anterior and medial	1	0	1	
Number of portals, n (%)				
2	36	16	20	0.687
3	7	4	3	

Abbreviations: UICC = International Union Against Cancer.
SD = standard deviation.

Table 2
Dose fractionation.

Total dose/ fractionation	Total (n = 43)	Larger enlargement group (n = 20)	Smaller enlargement group (n = 23)	BED (α/β = 10)
49.5 GyE/15 fr	1	1	0	65.8
54.0 GyE/15 fr	1	0	1	73.4
60.0 GyE/15 fr	2	0	2	84.0
66.0 GyE/15 fr	2	1	1	95.0
72.0 GyE/15 fr	3	1	2	106.6
79.5 GyE/15 fr	1	0	1	121.6
54.0 GyE/12 fr	1	0	1	78.3
60.0 GyE/12 fr	3	2	1	90.0
66.0 GyE/12 fr	2	2	0	102.3
69.6 GyE/12 fr	4	1	3	110.0
48.0 GyE/8 fr	2	0	2	76.8
52.8 GyE/8 fr	7	3	4	87.6
52.8 GyE/4 fr	14	9	5	122.5

Abbreviations: BED = biological effective dose.

The dose was calculated for the target volume and any nearby critical structures and expressed in Gray equivalents (GyE = carbon physical dose [in Gray] × relative biologic effectiveness). Radiobiologic studies were performed in mice and in five human cell lines cultured *in vitro* to estimate the relative biologic effectiveness values relative to megavoltage photons. Irrespective of the size of the spread-out Bragg peak (SOBP), the relative biologic effectiveness value of carbon ions was estimated as 3.0 at the distal part of the SOBP, and ridge filters were designed to produce a physical dose gradient of the SOBP so that the biologic effect along the SOBP became uniform. This was based on the biologic response of human salivary gland tumor cells at a 10% survival level.

CIRT was given at a total dose range of 48.0–79.5 GyE in 4–15 fractions. Ten patients were treated at a total dose range of 49.5–79.5 GyE in 15 fractions, 10 at 54.0–69.6 GyE in 12 fractions, 9 at 48.0–52.8 GyE in 8 fractions, and 14 at 52.8 GyE in four fractions. CIRT was administered once a day, four fractions per a week, and one port was used in each session. Double-field geometry was used for CIRT in 36 patients; for the remaining seven patients, three-field geometry was used (Tables 1 and 2).

Measurement of liver volume

The left lateral segment of the liver was defined as the non-irradiated region, and the other segments as irradiated. The AZE Company Workstation VIRTUAL PLACE ADVANCE PLUS liver analysis software was used for measuring liver volume. Liver contours (both irradiated and non-irradiated regions) and contours of the target tumors to be treated were entered on each of the CT slices taken prior to treatment and at 3, 6 and 12 months after CIRT, and the volume of the liver in the irradiated region (excluding the target tumor volume) as well as that in the non-irradiated region were measured. Since hepatic cirrhosis is noted in most cases as the background disease, and to exclude any impact of right lobe atrophy and left lobe enlargement through natural processes, the evaluation period was limited to 12 months after treatment.

Survival and evaluation of liver function

Overall survival was measured from the starting date of treatment until the date of death from any cause. Disease-free survival was measured from the starting date of treatment to the time of either death due to disease or of the first clinical or radiographic evidence of systemic or regional disease recurrence. We investigated the relationships between survivals and enlargement volume of the non-irradiated region at 3 months after CIRT. Patients with 50 cm^3 or greater enlargement volume of the non-irradiated region at 3 months post-treatment were classified as the larger enlargement group, and those with less than 50 cm^3 enlargement as the smaller enlargement group. Serial changes in serum albumin, prothrombin activity, total bilirubin level, and platelet count were reviewed before and 12 months after treatment in the larger and smaller enlargement groups.

Statistical analysis

Statistical analyses were performed using SPSS version 12.0 (SPSS Inc., Chicago, IL). Results were reported as mean ± standard deviation. For continuous variables, non-parametric tests (Friedman test, Wilcoxon's signed *r* rank test, and Mann–Whitney *U* test) were used. For categorical data, chi-squared test or Fisher's exact test was used. Prognostic factor analyses were performed using the Cox proportional hazards regression model. The Kaplan–Meier method was used for calculation of survival rates, and survival curves were compared by log-rank test. Multivariate analyses of factors related to enlargement of the non-irradiated region at 3 months after CIRT were performed using logistic regression analyses. Statistical significance was considered if $P < 0.05$ (*P*-values from two-sided tests), but for multiple comparisons of liver volume, Bonferroni's inequality was used.

Table 3
Changes in liver volume.

	Before	3 months after	6 months after	12 months after
Total (n = 43)				
Irradiated region (cm^3)	756.6 ± 134.1	696.1 ± 229.1	632.9 ± 164.2	575.9 ± 145.7
Volume variation (cm^3) (%)	−60.5 ± 204.3 (−7.8 ± 28.1)	−123.7 ± 145.7 (−15.9 ± 19.0)	−180.7 ± 104.2 (−24.0 ± 13.7)	
Non-irradiated region (cm^3)	320.0 ± 166.3	379.4 ± 169.4	389.5 ± 177.5	390.4 ± 185.7
Volume variation (cm^3) (%)	59.4 ± 80.4 (25.3 ± 37.2)	69.5 ± 85.3 (28.7 ± 36.6)	70.4 ± 85.2 (27.0 ± 33.9)	
Larger enlargement group (n = 20)				
Irradiated region (cm^3)	767.1 ± 138.1	726.7 ± 294.5	662.8 ± 178.8	582.7 ± 149.3
Volume variation (cm^3) (%)	−40.4 ± 279.8 (−4.7 ± 39.1)	−104.3 ± 177.7 (−12.7 ± 23.8)	−184.4 ± 111.9 (−24.1 ± 15.3)	
Non-irradiated region (cm^3)	317.2 ± 152.7	438.1 ± 152.0	444.9 ± 165.0	441.9 ± 162.7
Volume variation (cm^3) (%)	120.9 ± 74.1 (47.7 ± 42.6)	127.7 ± 84.0 (50.3 ± 40.5)		
Smaller enlargement group (n = 23)				
Irradiated region (cm^3)	747.5 ± 132.9	669.4 ± 154.1	606.9 ± 149.4	570.0 ± 145.7
Volume variation (cm^3) (%)	−78.1 ± 106.6 (−10.4 ± 13.2)	−140.6 ± 112.3 (−18.7 ± 13.6)	−177.5 ± 99.4 (−24.0 ± 12.4)	
Non-irradiated region (cm^3)	322.4 ± 180.6	328.3 ± 170.2	341.3 ± 177.3	345.6 ± 196.1
Volume variation (cm^3)(%)	5.9 ± 34.0 (5.8 ± 15.2)	18.9 ± 45.2 (10.0 ± 18.8)	23.2 ± 60.1 (9.6 ± 20.6)	

Values are given as mean ± standard deviation.

Results

The changes with time in liver volume values are shown in Table 3. In all patients, the volume of the irradiated region decreased significantly and that of the non-irradiated region increased significantly by the Friedman test ($P < 0.001$, $P < 0.001$, respectively), with the difference over time in the irradiated region by multiple comparisons showing that significant differences existed between any two time-points ($P < 0.001$, each). In the non-irradiated region, comparisons showed that significant differences existed between before treatment and 3, 6, and 12 months after treatment ($P < 0.001$, $P < 0.001$, $P < 0.001$, respectively), but there were no significant differences between 3 and 6 months, 3 and 12 months, and 6 and 12 months ($P = 0.091$, $P = 0.084$, and $P = 0.599$, respectively). Comparing the time-related changes of the liver volume in terms of the larger and smaller enlargement groups, both of the two groups showed significant atrophy of the irradiated region ($P < 0.001$, $P < 0.001$, respectively) and significant enlargement of the non-irradiated region ($P < 0.001$, $P = 0.022$, respectively) (Fig. 1). Further, the enlarged volume of the non-irradiated region 3 months after CIRT $\geqslant 50$ cm^3 was a prognostic factor (Table 4).

There were significant differences between the larger and smaller enlargement groups in overall survival rate and disease-free survival rate ($P = 0.030$, $P = 0.008$, respectively). Overall survival rates after 3 and 5 years were 80.0% (95% confidence interval [CI], 63–98) and 48.9% (95% CI, 27–71) in the larger enlargement group and 52.2% (95% CI, 32–73) and 29.4% (95% CI, 10–48) in the smaller enlargement group (Fig. 2a). Disease-free survival rates after 3 and 5 years were 50.0% (95% CI, 28–72) and 28.0% (95% CI, 7–49) in the larger enlargement group and 26.1% (95% CI, 8–44) and 0.0% (95% CI, 0–0) in the smaller enlargement group (Fig. 2b).

Table 5 shows the comparison of liver function between the two groups. Before treatment, there were no significant differences in serum albumin, prothrombin activity, and total bilirubin level between the two groups ($P = 0.659$, $P = 0.670$, and $P = 0.072$, respectively). Yet, 12 months after the treatment the larger enlargement group exhibited significantly higher serum albumin and prothrombin activity and lower total bilirubin levels than the smaller enlargement group ($P = 0.015$, $P = 0.002$, $P = 0.042$, respectively). As for platelet count, there were significant differences between the two groups before and after the treatment ($P = 0.002$, $P = 0.002$, respectively).

Univariate analysis showed that the planning target volume (PTV) and platelet count were significant factors for compensatory liver enlargement. Multivariate analysis showed only platelet count to be a significant factor (Table 6).

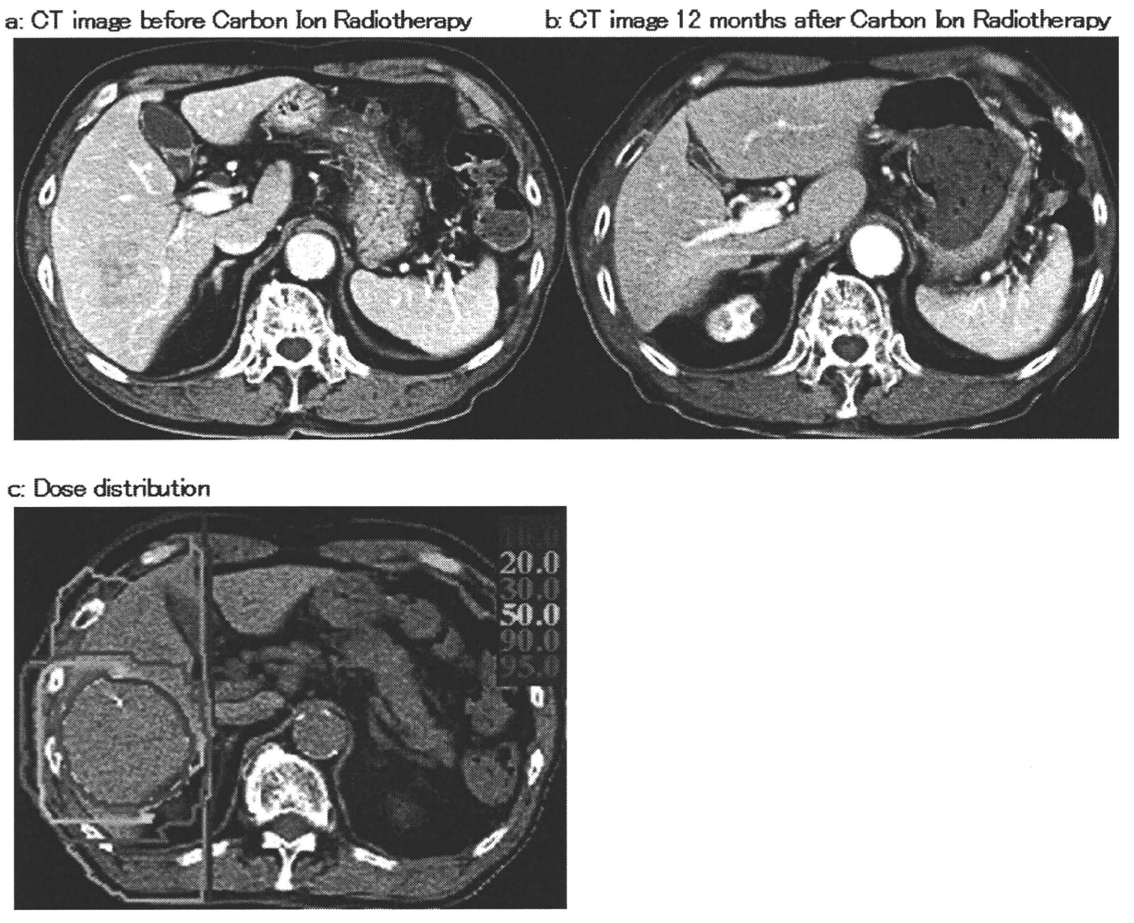

Fig. 1. CT images before and 12 months after carbon ion radiotherapy and dose distribution. CT image obtained in 81-year-old man from the larger enlargement group shows shrinkage of right hepatic lobe (840.5 cm^3 → 739.0 cm^3) and enlargement of left lateral segment (154.5 cm^3 → 266.4 cm^3). Hepatic function of this patient was retained. Serum albumin level before and 12 months after therapy was 4.5 and 4.0 g/dl, respectively. Prothrombin activity was 85.7% and 82.7%, respectively. Total bilirubin level was 0.7 and 0.7 mg/dl, respectively. Platelet count was 13.5 × 10^4 and 17.8 × 10^4/μl, respectively.

Table 4
Factors related to overall survival.

Factor	No. of patients	Univariate		Multivariate	
		Hazard ratio (95% CI)	P	Hazard ratio (95% CI)	P
Gender					
Male	29	1.00 (0.47–2.10)	0.994	0.55 (0.18–1.72)	0.305
Female	14				
Age (years)					
<65	15	1.12 (0.59–2.43)	0.614	1.82 (0.80–4.18)	0.155
⩾65	28				
Child-Pugh classification					
A	35	1.40 (0.63–3.10)	0.406	1.48 (0.45–4.85)	0.520
B	8				
Platelet count ($\times 10^4/\mu l$)					
<10	17	0.57 (0.29–1.15)	0.114	0.51 (0.20–1.33)	0.169
⩾10	26				
Enlargement volume of non-irradiated region at 3 months after CIRT (cm^3)					
<50	23	0.45 (0.22–0.94)	0.034	0.36 (0.15–0.88)	0.025
⩾50	20				
Planning target volume (cm^3)					
<200	24	0.78 (0.39–1.56)	0.489	1.51 (0.63–3.59)	0.357
⩾200	19				
Biological effective dose ($\alpha/\beta = 10$)					
Low (65.8–95.0)	19	0.81 (0.41–1.62)	0.555	0.95 (0.41–2.20)	0.912
High (102.3–122.5)	24				
Number of tumors					
1	36	1.07 (0.44–2.61)	0.881	0.50 (0.16–1.54)	0.226
2	7				

Discussion

In the present study, we have shown that cases with irradiation of the right lobe of the liver develop enlargement of the left lateral segment by way of compensation after CIRT and that the compensatory enlargement is contributory to the improvement of prognosis.

Approximately 80% of all HCC patients have chronic liver disorders [3], which require effective and necessarily minimally invasive therapy of HCC. We have reported that CIRT appears safe and effective for patients with HCC [22,23]. However, the reason why liver function is retained despite atrophy of the irradiated region of the liver still remained to be investigated. Hemming et al. reported that preoperative portal vein embolization performed in extended hepatectomy cases caused enlargement of the remnant liver [28]. In other research studies, enlargement of the remnant liver has been shown to have the effect of improving liver function [32–34]. Moreover, after radiotherapy, veno-occlusive diseases of the liver occur, which, it is argued, are the cause of radiation-induced liver disease [35–37]. From the above, we wonder whether the same mechanism might hold true for CIRT.

In this study, we measured the volumes of the irradiated and non-irradiated regions using CT imaging. Heymsfield and associates first measured the volume of a cadaver's liver using CT in 1979, showing that the discrepancy between the volume measured by CT and that measured using the water replacement method was

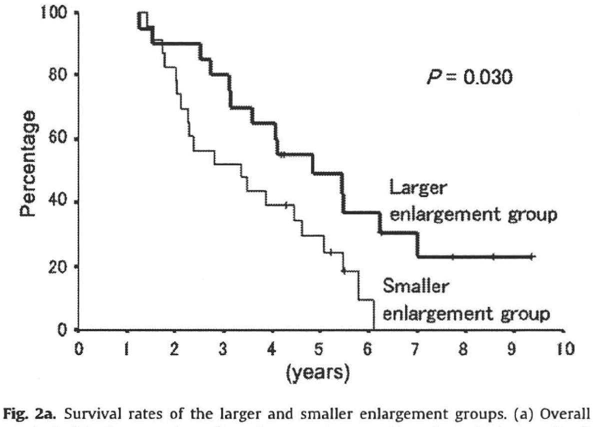

Fig. 2a. Survival rates of the larger and smaller enlargement groups. (a) Overall survival of the larger and smaller enlargement groups. Overall survival rates after 3 and 5 years were 80.0% (95% confidence interval [CI], 63–98) and 48.9% (95% CI, 27–71) in the larger enlargement group and 52.2% (95% CI, 32–73) and 29.4% (95% CI, 10–48) in the smaller enlargement group.

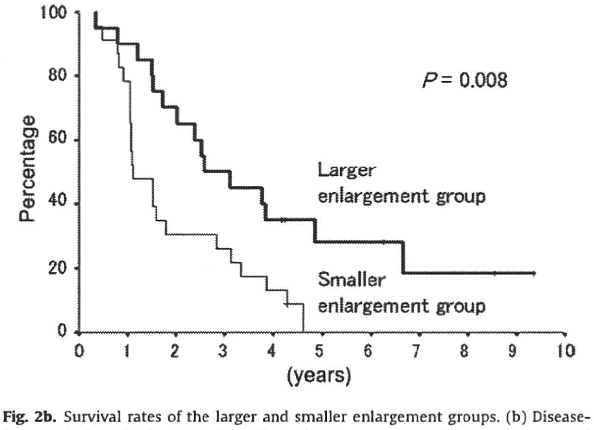

Fig. 2b. Survival rates of the larger and smaller enlargement groups. (b) Disease-free survival of the larger and smaller enlargement groups. Disease-free survival rates after 3 and 5 years were 50.0% (95% CI, 28–72) and 28.0% (95% CI, 7–49) in the larger enlargement group and 26.1% (95% CI, 8–44) and 0.0% (95% CI, 0–0) in the smaller enlargement group.

Table 5
Comparison of liver function.

	Before			12 months after		
	Larger enlargement group (*n* = 20)	Smaller enlargement group (*n* = 23)	*P*	Larger enlargement group (*n* = 20)	Smaller enlargement group (*n* = 23)	*P*
Albumin (g/dl)	3.9 ± 0.4	3.8 ± 0.4	0.659	3.9 ± 0.3	3.7 ± 0.4	0.015
Prothrombin activity (%)	78.6 ± 11.4	76.0 ± 15.3	0.670	81.9 ± 9.3	69.7 ± 11.9	0.002
Total bilirubin (mg/dl)	0.9 ± 0.3	1.1 ± 0.4	0.072	0.9 ± 0.5	1.1 ± 0.4	0.042
Platelet count (×10^4/μl)	14.0 ± 4.3	9.9 ± 3.9	0.002	14.6 ± 7.9	8.5 ± 3.4	0.002

Values are given as mean ± standard deviation.

Table 6
Factors related to compensatory enlargement.

Factor	No. of patients	Univariate *P*	Multivariate *P*	Hazard ratio	95% Confidence interval
Planning target volume (PTV) (cm³)					
<200	24	0.013	0.147	2.92	0.69–12.46
⩾200	19				
Platelet count (×10⁴/μl)					
<10	17	0.004	0.028	5.85	1.21–28.31
⩾10	26				
Biological effective dose (BED) (α/β = 10)					
Low (65.8–95.0)	19	0.261	0.479	1.67	0.40–6.94
High (102.3–122.5)	24				

within 5% [38]. In 1981, Moss et al. also measured liver volume using CT, confirming the conclusion of Heymsfield et al. [39]. Many studies have reported that the difference between CT-measured liver volume and the actual liver volume is minor [38–40]. In our study, the volume of the left lateral segment was 320.0 ± 166.3 cm^3 (Table 3). Zhou et al. measured the volume of 113 hepatic lobes using CT. They reported average volumes of the left lateral segment of 313.2 ± 105.1 and 282.2 ± 136.2 cm^3 in Child-Pugh class A and B patients, respectively [41]. These results generally resemble ours, lending support to the accuracy and reliability of our measuring method.

It is difficult to distinguish strictly the irradiated and non-irradiated portions, and therefore in this study we defined the left lateral segment of the liver as the non-irradiated region, and the other segments as irradiated. In 11 of 43 patients, the region considered as irradiated was larger than the region really receiving radiation. We cannot examine whether the non-irradiated portions of the right lobes enlarge or not because it is difficult to distinguish the irradiated and non-irradiated portions of the right lobe. The volumes of the irradiated part of the liver measured at 0, 3, 6, and 12 months after treatment, respectively, did show significant differences. With the lapse of time, the measurement values decreased significantly. In contrast, the liver volumes of the non-irradiated part increased at 3 months post-treatment on a significant scale compared to before the treatment. From then on, no more significant increases were observed. These data demonstrate that the enlargement of the non-irradiated region is not a matter of the natural course associated with chronic liver disorders, but rather results as compensation for the CIRT-caused atrophy of the liver.

We divided the subjects into two groups according to compensatory enlargement liver volume of more or less than 50 cm^3 because enlarged volume of the non-irradiated region 3 months after CIRT ⩾50 cm^3 was a prognostic factor. In terms of liver function, many complex methods for estimating liver functional reserve have been advocated, including tests that measure liver metabolic activity such as ICG clearance, galactose elimination, and aminopyrine clearance [42]. However, it was demonstrated that either one of Child classification [43] or Okuda staging [44] is highly predictive for outcome [45]. Serum albumin, prothrombin activity, and total bilirubin level are the serum items of the Child-Pugh score, which is the index of hepatic functional reserve. Therefore, Serial changes in these items were reviewed as hepatic functional reserve before and 12 months after treatment in the two groups. There were no significant differences in them before the treatment, but at 12 months after, the larger enlargement group remained significantly more favorable than the smaller enlargement group. On the other hand, the extent of atrophy of the irradiated regions was found to be significantly similar in the two groups. These data indicate the possibility that the compensatory enlargement, taking place in the non-irradiated region of the liver after CIRT, affect hepatic functional reserve. It was suggested that better disease-free survival and hepatic functional reserve contributed to improvement of overall survival.

We investigated PTV, platelet count, and biological effective dose (BED) as indicators of enlargement of the non-irradiated region at 3 months after CIRT. PTV and platelet count were selected on the basis of their significant differences between the larger and smaller enlargement groups. In our study, it was difficult to compare the differences of total dose and fractionations because of their various combinations. Then, although it has not been confirmed that BED is adaptable to CIRT, we tried to calculate BED for every fractionation by L/Q model [46], adding it to the variables. The difference in mean age between the two groups was thought not to be related to the compensatory enlargement of the liver after CIRT, based on the self-evident discrepancy between age and the enlargement volume, i.e., the higher the age, the larger the volume. Therefore, we excluded age from the analysis of the indicators of compensatory enlargement of the non-irradiated liver. Our data demonstrated platelet count to be the major factor of compensatory enlargement of the non-irradiated liver, and it is known that platelet count decreases in parallel with the grade of chronic liver disease [47]. Thus, we intend to investigate the relationship between liver fibrosis and compensatory enlargement of the liver in future studies.

Considering the limitations of this study, we must first point out the nature of the investigation as a retrospective one. Secondly, the subjects were restricted to cases in which target tumors were located in the right lobe of the liver. Thirdly, we did not utilize any biochemical or molecular biological method.

It was demonstrated that the non-irradiated region of the liver enlarged compensatively until 3 months after CIRT and that the enlarged volume of this region 3 months after CIRT ⩾50 cm^3 was a prognostic factor. We can conclude that compensatory enlargement of the non-irradiated liver contributes to the improvement of prognosis.

Conflict of interest statement

Any actual or potential conflicts of interest do not exist.

Acknowledgments

This study was supported by the Research Project with Heavy Ions of the National Institute of Radiological Sciences in Japan. We are grateful to members of the National Institute of Radiological Sciences. We are indebted to Dr. Gen Kobashi and Dr. Kaori Ohta for statistical support.

References

[1] Bosch FX, Ribes J, Borras J. Epidemiology of primary liver cancer. Semin Liver Dis 1999;19:271–85.
[2] Marugame T, Matsuda T, Kamo K, et al. Cancer incidence and incidence rates in Japan in 2001 based on the data from 10 population-based cancer registries. Jpn J Clin Oncol 2007;37:884–91.
[3] Ikai I, Arii S, Okazaki M, et al. Report of the 17th Nationwide Follow-up Survey of Primary Liver Cancer in Japan. Hepatol Res 2007;37:676–91.
[4] Mulcahy MF. Management of hepatocellular cancer. Curr Treat Options Oncol 2005;6:423–35.
[5] Kuvshinoff BW, Ota DM. Radiofrequency ablation of liver tumors: influence of technique and tumor size. Surgery 2002;132:605–11.
[6] Shiina S, Teratani T, Obi S, et al. A randomized controlled trial of radiofrequency ablation with ethanol injection for small hepatocellular carcinoma. Gastroenterology 2005;129:122–30.
[7] Sato M, Watanabe Y, Ueda S, et al. Microwave coagulation therapy for hepatocellular carcinoma. Gastroenterology 1996;110:1507–14.
[8] Camma C, Schepis F, Orlando A, et al. Transarterial chemoembolization for unresectable hepatocellular carcinoma: meta-analysis of randomized controlled trials. Radiology 2002;224:47–54.
[9] Lo CM, Ngan H, Tso WK, et al. Randomized controlled trial of transarterial lipiodol chemoembolization for unresectable hepatocellular carcinoma. Hepatology 2002;35:1164–71.
[10] Llovet JM, Real MI, Montana X, et al. Arterial embolization or chemoembolization versus symptomatic treatment in patients with unresectable hepatocellular carcinoma: a randomized controlled trial. Lancet 2002;359:1734–9.
[11] Higuchi T, Kikuchi M, Okazaki M. Hepatocellular carcinoma after transcatheter hepatic arterial embolization. A histopathologic study of 84 resected cases. Cancer 1994;73:2259–67.
[12] Adachi E, Matsumata T, Nishizaki T, Hashimoto H, Tsuneyoshi M, Sugimachi K. Effects of preoperative transcatheter hepatic arterial chemoembolization for hepatocellular carcinoma. The relationship between postoperative course and tumor necrosis. Cancer 1993;72:3593–8.
[13] Phillips R, Murikami K. Preliminary neoplasms of the liver. Results of radiation therapy. Cancer 1960;13:714–20.
[14] Stillwagon GB, Order SE, Guse C, et al. 194 hepatocellular cancers treated by radiation and chemotherapy combinations: toxicity and response: a Radiation Therapy Oncology Group study. Int J Radiat Oncol Biol Phys 1989;17:1223–9.
[15] Zhao JD, Xu ZY, Zhu J, et al. Application of active breathing control in 3-dimensional conformal radiation therapy for hepatocellular carcinoma: the feasibility and benefit. Radiother Oncol 2008;87:439–44.
[16] Toya R, Murakami R, Baba Y, et al. Conformal radiation therapy for portal vein tumor thrombosis of hepatocellular carcinoma. Radiother Oncol 2007;84:266–71.
[17] Robertson JM, Lawrence TS, Dworzanin LM, et al. Treatment of primary hepatobiliary cancers with conformal radiation therapy and regional chemotherapy. J Clin Oncol 1993;11:1286–93.
[18] Suit HD, Goitein M, Munzenrider J, et al. Increased efficacy of radiation therapy by use of proton beam. Strahlenther Onkol 1990;166:40–4.
[19] Matsuzaki Y, Osuga T, Saito Y, et al. A new, effective, and safe therapeutic option using proton irradiation for hepatocellular carcinoma. Gastroenterology 1994;106:1032–41.
[20] Kanai T, Endo M, Minohara S, et al. Biophysical characteristics of HIMAC clinical irradiation system for heavy-ion radiation therapy. Int J Radiat Oncol Biol Phys 1999;44:201–10.
[21] Kanai T, Furusawa Y, Fukutsu K, Itsukaichi H, Eguchi-Kasai K, Ohara H. Irradiation of mixed beam and design of spread-out Bragg peak for heavy-ion radiotherapy. Radiat Res 1997;147:78–85.
[22] Kato H, Tsujii H, Miyamoto T, et al. Results of the first prospective study of carbon ion radiotherapy for hepatocellular carcinoma with liver cirrhosis. Int J Radiat Oncol Biol Phys 2004;59:1468–76.
[23] Kato H, Yamada S, Yasuda S, et al. Phase II study of short-course carbon ion radiotherapy (52.8GyE/4-fraction/1-week) for hepatocellular carcinoma. Hepatology 2005;42(Suppl. 1):381A.
[24] Blakely EA, Ngo FQH, Curtis SB, et al. Heavy ion radiobiology: cellular studies. Adv Radiat Biol 1984;11:295–378.
[25] Castro JR. Future research strategy for heavy ion radiotherapy. In: Kogelnih HD, editor. Progress in radio-oncology. Bologna: Monduzzi Editore; 1995. p. 643–8.
[26] Tsujii H, Morita S, Miyamoto T, et al. Preliminary results of phase I/II carbon ion therapy. J Brachyther Int 1997;13:1–8.
[27] Suzuki M, Kase Y, Yamaguchi H, Kanai T, Ando K. Relative biological effectiveness for cell-killing effect on various human cell lines irradiated with heavy-ion medical accelerator in Chiba (HIMAC) carbon-ion beams. Int J Radiat Oncol Biol Phys 2000;48:241–50.
[28] Hemming AW, Reed AI, Howard RJ, et al. Preoperative portal vein embolization for extended hepatectomy. Ann Surg 2003;237:686–91.
[29] Abulkhir A, Limongelli P, Healey AJ, et al. Preoperative portal vein embolization for major liver resection: a meta-analysis. Ann Surg 2008;247:49–57.
[30] Sato K, Yamada H, Ogawa K, et al. Performance of HIMAC. Nucl Phys 1995;A588:229–34.
[31] Minohara S, Kanai T, Endo M, Noda K, Kanazawa M. Respiratory gated irradiation system for heavy-ion radiotherapy. Int J Radiat Oncol Biol Phys 2000;47:1097–103.
[32] Kubo S, Shiomi S, Tanaka H, et al. Evaluation of the effect of portal vein embolization on liver function by (99m)tc-galactosyl human serum albumin scintigraphy. J Surg Res 2002;107:113–8.
[33] Kudo M, Todo A, Ikekubo K, Yamamoto K, Vera DR, Standalnik RC. Quantitative assessment of hepatocellular function through in vivo radioreceptor imaging with technetium 99m galactosyl human serum albumin. Hepatology 1993;17:814–9.
[34] Vera DR, Topcu SJ, Stadalnik RC. In vitro quantification of asialoglycoprotein receptor density from human hepatic microsamples. Methods Enzymol 1994;247:394–402.
[35] Reed Jr GB, Cox Jr AJ. The human liver after radiation injury. A form of veno-occlusive disease. Am J Pathol 1966;48:597–611.
[36] Lawrence TS, Robertson JM, Anscher MS, Jirtle RL, Ensminger WD, Fajardo LF. Hepatic toxicity resulting from cancer treatment. Int J Radiat Oncol Biol Phys 1995;31:1237–48.
[37] Cheng JC, Wu JK, Huang CM, et al. Radiation-induced liver disease after radiotherapy for hepatocellular carcinoma: clinical manifestation and dosimetric description. Radiother Oncol 2002;63:41–5.
[38] Heymsfield SB, Fulenwider T, Nordlinger B, Barlow R, Sones P, Kutner M. Accurate measurement of liver, kidney, and spleen volume and mass by computerized axial tomography. Ann Intern Med 1979;90:185–7.
[39] Moss AA, Friedman MA, Brito AC. Determination of liver, kidney, and spleen volumes by computed tomography: an experimental study in dogs. J Comput Assist Tomogr 1981;5:12–4.
[40] Sakamoto S, Uemoto S, Uryuhara K, et al. Graft size assessment and analysis of donors for living donor liver transplantation using right lobe. Transplantation 2001;71:1407–13.
[41] Zhou XP, Lu T, Wei YG, Chen XZ. Liver volume variation in patients with virus-induced cirrhosis: findings on MDCT. AJR Am J Roentgenol 2007;189:W153–159.
[42] Friedman LS, Martin P, Santiago JM. Liver function tests and the objective evaluation of the patient with liver disease. In: Zakim D, Boyer TD, editors. Hepatology. Philadelphia: WB Saunders; 1996. p. 791–833.
[43] Wants GE, Payne MA. Experience with portacaval shunt for portal hypertension. N Engl J Med 1961;265:721–8.
[44] Okuda K, Ohtsuki T, Obata H, et al. Natural history of hepatocellular carcinoma and prognosis in relation to treatment. Cancer 1985;56:918–28.
[45] Fong Y, Sun RL, Jarnagin W, et al. An analysis of 412 cases of hepatocellular carcinoma at a western center. Ann Surg 1999;229:790–9.
[46] Lee SP, Leu MY, Smathers JB, et al. Biologically effective dose distribution based on the linear quadratic model and its clinical relevance. Int J Radiat Oncol Biol Phys 1995;33:375–89.
[47] Karasu Z, Tekin F, Ersoz G, et al. Liver fibrosis is associated with decreased peripheral count in patients with chronic hepatitis B and C. Dig Dis Sci 2007;52:1535–9.